E877 Note # SUNYSB-96-003

September 30, 1996

Proton and Pion Production Relative to the Reaction Plane in $Au + Au$ Collisions at 10.8 GeV

Wen-Chen Chang

State University of New York, Stony Brook, NY 11794-3800

and

Sergei A. Voloshin

University of Heidelberg, Heidelberg, Germany, and MEPI, Moscow, Russia

ABSTRACT

The results of detailed analysis of proton and charged pion azimuthal distributions measured with respect to the reaction plane in $Au + Au$ collisions at 10.8 GeV/c are presented. Azimuthal anisotropy is studied as a function of rapidity and transverse momentum of the particles for different centralities of the collision. The triple differential (in rapidity, transverse momentum, and azimuthal angle) distributions are reconstructed. The comparison of the results with previous analysis of charged particle and transverse energy flow as well as with model predictions are presented.

I. INTRODUCTION

In this note we present the results of analysis of anisotropic transverse collective flow of identified particles, namely protons and charged pions, detected by E877 spectrometer in $Au + Au$ collisions at 10.8 GeV/c. The data were taken during 1993 Fall run.

Anisotropic flow has been first observed at BNL AGS energies by E877 Collaboration [1] by the method [4], which involves Fourier analysis of azimuthal distributions on event-by-event basis. This method does not require the reconstruction of the reaction plane, but does require a big number of particles in each (pseudo)rapidity bin under study. Due to this limitation the method cannot be applied for the study of flow using spectrometer data. But the knowledge, that anisotropic flow is present in the collisions, justifies the explicit reconstruction of the reaction plane event by event, and the analysis of event shape with respect to this plane. The analysis of charged multiplicity and transverse energy flow was performed in this way in [2]. Now we apply a similar procedure to determine the triple differential multiplicities $d^3N/(dp'_x dp'_y dy)$ of identified proton and charged pions. Here and below we denote by prime the values in the coordinate system defined by the reaction plane. For example, the azimuthal angle in this system we denote as $\phi' = \phi - \Psi_r$, where Ψ_r is the reaction plane angle in the laboratory fixed frame.

This note is organized as following. First we describe the whole procedure of the analysis. Many of technical details are put in the Appendixes. We present first the results on Fourier analysis of particle azimuthal distributions in different rapidity bins and for different centralities of the collision. These results are to a large extent independent from the uncertainties in spectrometer efficiency and the detector acceptance. Then the results on triple differential multiplicities and related quantities (such as $\langle p_x \rangle$) are discussed. Different flow scenarios are discussed from the point of view of the observed dependence of flow signal on transverse momentum (p_t) of the particles. We also compare our measurements with our estimates of proton and pion flow from charged multiplicity and transverse energy flow [2], as well as with model (RQMD 2.3 [5]) prediction. Finally we summarize our results.

II. STRUCTURE OF THE ANALYSIS

The structure of the analysis is very similar to the one used in [2], and many details can be found there. We study the azimuthal anisotropy of particle production by means of Fourier analysis. Namely we study the rapidity, transverse momentum, and centrality dependence of Fourier coefficients v_n in the decomposition:

$$E\frac{d^3N}{d^3p} = \frac{d^3N}{p_t dp_t dy d\phi'} = \frac{1}{2\pi}\frac{d^2N}{p_t dp_t dy}(1 + 2v_1\cos(\phi') + 2v_2\cos(2\phi') + 2v_3\cos(3\phi') + ...). \quad (1)$$

In each event the reaction plane angle is determined by the direction of transverse energy flow in Target and Participant calorimeters, and the transverse coordinate system is redefined to make the reaction plane to be the new $x-z$ plane. Note that the coverage of the calorimeters, used for the reaction plane determination, does not overlap with the spectrometer coverage, and thus in this analysis we are free from the problems related to autocorrelations. The p_x and p_y of identified particles in each event are mapped into the new coordinate system and the particle distributions are determined with respect to the reaction plane. We have full 2π acceptance only for very limited p_t range ($p_t \leq 100$ MeV), but the triple differential multiplicity is constructed in full taking into account 2π range of the reaction plane angle distribution.

Similarly to the analysis [2] the reaction plane angle is determined in four independent pseudo-rapidity windows. The reaction plane resolution is evaluated by studying the correlation between flow angles determined in different windows. Then the flow signals are corrected for this resolution. Details of this procedure are described in [2]. Due to a very small azimuthal coverage of the spectrometer a special precaution is taken to get the reaction plane angle distribution as flat as possible (see Appendix A). Even though the flatness of the reaction plane distribution gets significant improvement after the procedure described in Appendix A, the residual non-flatness might be not negligible, when the flow signal is small. In Appendix B we demonstrate how the non-flatness of the reaction plane angle distribution propagates to the measured anisotropy and the way to correct for it.

In E877 setup charged particles emitted in the forward direction and passed through the collimator ($-134 < \theta_{horizontal} < 16$ mrad, $-11 < \theta_{vertical} < 11$ mrad) are analyzed by the magnetic spectrometer. Tracks are reconstructed by the hits in two high resolution drift chambers (DCII and DCIII) and four multi-wire proportional chambers (MWPC). The average momentum resolution is $\Delta p/p \approx 4\%$. Time-of-Flight hodoscope located behind the tracking chambers provides the time of flight with approximately 85 ps resolution.

Flow of different particles might be very different in both magnitude and sign. A small admixture in the particle sample of other particle species could heavily bias the final results. Due to this reason, in the current analysis more strict requirements are applied for particle identification than, for example, in [3]. For example, in *momentum vs mass squared* plot we select only hits in the region of $1.5\,\sigma$ around m^2 peak and reject everything what belongs to $3\,\sigma$ region of other particles. The details of the particle identification are presented in Appendix C.

The Fourier coefficients of azimuthal distributions evaluated by the procedure described above are corrected for the reaction plane resolution, and are independent of the detector acceptance. Combined with the measurements [3] of p_t and rapidity spectra they provide the triple differential distributions in y, p_t, and ϕ' (see formula (1)). Independently from the analysis [3] we also reconstruct the triple differential distributions directly from the data. For this purpose we have to understand how to correct for the tracking efficiency due to the occupancy and the detector acceptance. The details of this calculations are presented in Appendix D.

III. RESULTS

A. Directed Flow

We quantify directed flow by v_1 the first coefficient in Fourier decomposition of azimuthal particle distribution. After weighted with p_t this coefficient yields widely used quantity $\langle p_x \rangle$ the mean value of transverse momentum projected onto the reaction plane.

$$\langle p_x \rangle = \frac{1}{N} \int \frac{dN}{dp_t} (v_1 \cdot p_t) dp_t \qquad (2)$$

We would like to emphasise, that $\langle p_x \rangle$, as any other integral quantity, is less informative in comparison with v_1. For example, v_1 dependence on p_t is different for different flow scenarios and can be used as a guidance to choose the appropriate one (see below).

The coefficient v_1 is analyzed as a function of transverse momentum for different rapidity and centrality bins of the collision. Three centrality regions, selected in accordance to PCal E_T: $200 < E_T < 230$, $230 < E_T < 270$, and $E_T > 270$ GeV, correspond to (see Fig. 4 in [2]) the values of $\sigma_{top}/\sigma_{geo}$ approximately 13–9%, 9–4%, and <4%, respectively.

In Fig. 1, the contour plot of the triple differential multiplicity of proton and charged pions measured with respect to the reaction plane (xz plane) are shown in the rapidity slice $3.0 < y < 3.1$. The overall shift of proton distribution toward positive p_x is obvious. Charged pions slightly move in the opposite direction (negative p_x). The distributions shown are not corrected for the reaction plane resolution.

The results of directed flow signal v_1 corrected for the reaction plane resolution are presented in Figures 2–4 for protons and charged pions. Proton production is very strongly correlated with the orientation of the reaction plane. Protons of larger p_t have larger value of v_1 with tendency to saturation in the highest p_t region. The largest value of v_1 is about 0.3 what corresponds to the high p_t proton yield change almost in 4 times from $\phi' = \pi$ to $\phi' = 0$. Note that for the lowest centrality region protons with very small transverse momentum have a tendency to flow in opposite direction. This could be an indication of transverse isotropic expansion and should be studied in details using high statistics of '94 data.

Positive and negative pions behave very similar. Both of them exhibit small "anti-flow". Note very different behavior of proton and pion signals as a function of p_t. For protons v_1 grows almost linearly with p_t; for pions there is almost no p_t dependence with an average value about $v_1^\pi \approx -0.03$. (π^+ of smaller p_t seems to have bigger azimuthally anisotropic effect).

Centrality dependence of all flow signals is well pronounced. v_1^π becomes more positive toward central collision.

Note that independent of flow scenario $v_1(p_t)$ must vanish at $p_t = 0$, due to continuity of the spectra. This fact can be used for an estimate of a systematic error in the results of the analysis.

As was already mentioned, the another way of study of directed (sideward) flow is the evaluation of the mean projection of the transverse momentum onto the reaction plane $\langle p_x \rangle$

as a function of rapidity y. Our results for centrality region of exclusive top 10% geometrical cross section, shown in the Fig. 5, cover mostly the forward rapidity region. Due to the limited p_t acceptance the reliable evaluation of this quantity is possible only in rather small region of rapidity. For rapidities $y < 2.4$ we have to extrapolate v_1 in high p_t region and use thermal parameterization of proton p_t spectra (see also next section).

Anisotropic flow can be also characterized by the inverse slope of p_t spectra of particles emitted at different azimuthal angles. We extract this slope by fitting the spectra in high p_t region by thermal (Boltzmann) function with the slope parameter T_B, which depends on the azimuthal angle ϕ':

$$\frac{d^3N}{p_t\,dp_t\,dy\,d\phi'} = N_0(y)\,m_t \exp\left(-\frac{m_t - m}{T_B(\phi')}\right) \tag{3}$$

The results of this fit are shown in Fig. 7, where T_B is plotted as a function of the azimuthal emission angle.

B. Higher Harmonics in Azimuthal Distributions

Higher harmonics (v_2 and v_3) are also analyzed in the particle azimuthal distributions. The accuracy in the evaluation of the contribution of higher harmonics deteriorates with increasing harmonic order due to the limited reaction plane resolution (see the discussion in [2]). That results in larger relative errors. We do not observe any strong dependence of v_2 and v_3 on the transverse momentum (see Fig. 8 – Fig. 13) for different particle rapidities and centralities of the collision. Note that the positive value of v_2 corresponds to an elliptic-shaped distribution with the major axis in the reaction plane. The negative value of v_3 corresponds to the enhanced particle production at azimuthal angle values of $\phi' = \pi/3$, π, and $5\pi/3$.

IV. DISCUSSION

A. Moving Thermalized Source *vs* Absorption

Here we discuss the hypothesis if transverse anisotropic flow is a result of a transverse movement of the thermalized particle source. We start with the source being at rest and with the case of no transverse expansion.

In this case the particle invariant spectra are described by the formula:

$$\frac{1}{m_t}\frac{dN}{dm_t dy d\phi'} \propto E^* e^{-E^*/T}, \tag{4}$$

where T is the temperature, and E^* is the particle energy in the source rest frame.

Then we assume that the source moves along the x axis with velocity β_x (which we would call anisotropic transverse velocity, to distinguish from the velocity β_T of isotropic transverse expansion). In order to get the value of E^* one can use the Lorentz transformations:

$$E^* = E\cosh(y_t) - p_t \sinh(y_t)\cos(\phi') \approx E - p_t\beta_x \cos(\phi') \tag{5}$$

(where energy E is evaluated in the system moving longitudinally with the same velocity as the source $E = m_t \cosh(y - y^*)$).

We also assume that $\beta_x \ll 1$. The invariant particle distribution now reads:

$$\frac{1}{m_t}\frac{dN}{dm_t dy d\phi'} \propto E e^{-E/T}(1 - \frac{p_t\beta_x}{E}\cos(\phi') + \frac{p_t\beta_x}{T}\cos(\phi')) \propto (1 + 2v_1\cos(\phi')) \tag{6}$$

It follows that:

$$v_1 \approx \frac{p_t\beta_x}{2T}\left(1 - \frac{T}{m_t\langle\cosh(y - y^*)\rangle}\right). \tag{7}$$

For protons $E \gg T$ and the extraction of source velocity is straitforward.

In the case of not negligible transverse (isotropic) expansion the relations become more complicated, but the general behavior remains the same. The magnitude of directed flow (v_1) in high p_t region is almost directly proportional to β_x, but the slope depends now on the inverse slope parameter T_B, instead of the real temperature of the source. It reads:

$$v_1 \approx \frac{\beta_x}{2T_B}p_t. \tag{8}$$

Taking the data on v_1 for protons from Fig. 2 and $T_B \approx 100$ MeV [3] for the rapidity region close to the beam rapidity one gets the values of $\beta_x \approx 0.04$–0.06. In fig. 6, the extracted β_x of the proton source are shown for different proton rapidities and collision centralities.

For pions we observe v_1 with almost now dependence on p_t. It means that the physics of such flow is different from the moving source (just as one could expect). The possible explanation of pion flow signal would be an absorption in nuclear matter. For pions produced somewhere in the center of the collision and moving in the forward direction with the velocity close to the speed of light one would expect more nuclear matter from the direction of flow (positive x' in our system) and, consequently, more absorption. An assumption on independence of the absorption cross section on pion p_t would explain the observed v_1 behavior. In more central collisions pons exhibit less absorption in the spectator nucleons and more re-scattering with participant nucleons This results in more positive values of v_1.

Both for protons and pions we observe small but non zero v_3. It has negative values. It also finds an explanation in the re-scattering and/or absorption in comoving hadron matter.

B. Parameterization of d^3N/d^3p'

We use two functional forms to parameterize d^3N/d^3p' in each rapidity bin considered:

$$\Phi_1(p'_x, p'_y) \sim \frac{dN}{dy} \exp\left(-\frac{\sqrt{(p'_x - \langle p_x \rangle)^2 + p'^2_y + m^2}}{T}\right) \tag{9}$$

$$\Phi_2(p'_x, p'_y) \sim \frac{dN}{dy} \exp\left(-\frac{(p'_x - \langle p_x \rangle)^2}{2\sigma^2_{p_x}} - \frac{p'^2_y}{2\sigma^2_{p_y}}\right) \tag{10}$$

The parameters in function Φ_1 are: $\langle p_x \rangle$ and T; and in function Φ_2: $\langle p_x \rangle$, σ_{p_x}, and σ_{p_y}. The possible behavior of v_1 as a function of p_t for different sets of parameters corresponding to these functions is shown in Fig. 14. We use these function to fit the experimental values of $v_1(p_t)$ (see Fig. 15). The extracted values of $\langle p_x \rangle$ are shown in Fig. 16.

We also use the maximum likelihood fitting technique to make a 2d fit in each rapidity slice. The results of this fit were used for Fig. 5.

C. Comparison with the results on N_{ch} and E_T flow

Mapping the disentangled nucleon flow($v_1^{E_t(\eta)}$) into rapidity and assuming $v_1^{E_t(y)}$ to be close to $v_1^{p_t(\eta)}$, we get $\langle p_x \rangle$ in the region around mid-rapidity of Fig 5.

$$\langle p_x \rangle = v_1^{p_t(y)} (\approx v_1^{E_t(y)}) * \langle p_t \rangle \tag{11}$$

D. Comparison with RQMD 2.3

The comparison with RQMD 2.3 are shown. There are two modes: cascade and mean field. (Wait for Heinz Sorge to give us the RQMD 2.3)

V. SUMMARY AND CONCLUSION

The measured flow signals of identified particles show that protons (nucleons) exhibit strong directed flow and pions flow in the opposite direction in the mid-central collision. This is consistent with the observation in the measurement of E_T and N_{ch} flow within complementary acceptance([[2]]).

The linear dependence of the first Fourier moment of proton distribution on p_t can be interpreted in the picture of a transversely boosted thermal source. The boosting velocity β_x appeared to be about 0.1 around beam rapidity in mid-central collision.

The negative v_1 and much lesser p_t dependence for pions could be a results of pion absorption by the cold spectator nucleons. Some growth of pion v_1 with centrality of the collision reflects less absorption by spectators and more re-scattering on the participant nucleons.

Comparison with RQMD is coming.

APPENDIX

A. Flattening of the Reaction Plane Distribution

The reaction plane angle is defined by the direction of transverse energy flow in some pseudo-rapidity window. Due to the possible wrong gains and dead towers in the calorimeters the reconstructed reaction plane distribution generally is not flat. The effect is larger for PCAL windows as compared to TCAL. We apply the following procedures to correct for this non-flatness of the distribution. (It is important to remember that if due to the correction the shift of center of the distribution is not small then it affects also higher harmonics in the distribution and the use of method 2 can be required)

Method 1 (used for '93 ntuples production)

The distribution of uncorrected directivity vector in each centrality bin is fitted with a five-parameter function $F(E_x, E_y)$ by the maximum likelihood method.

$$E'_x = E_x - E_{x0} \tag{12}$$

$$E'_y = E_y - E_{y0} \tag{13}$$

$$E''_x = E'_x \cos(\phi_0) + E'_y \sin(\phi_0) \tag{14}$$

$$E''_y = E'_y \cos(\phi_0) - E'_x \sin(\phi_0) \tag{15}$$

$$F(E_x, E_y) = N_0 \exp(-(\frac{E''^2_x}{\delta^2_x} + \frac{E''^2_y}{\delta^2_y})) \tag{16}$$

$$\tag{17}$$

The five parameters $E_{x0}, E_{y0}, \phi_0, \delta_x,$ and δ_y stand for the center, the orientation and the widths of this assumed 2d elliptic-shape distribution. Then the vector $(E''_x/\delta_x, E''_y/\delta_y)$ defines new value of the reaction plane angle.

Method 2 (used in the '93 data analysis and for '94 ntuples production)

The another possible procedure to flatten the reaction plane angle distribution could be the following. Any flattening of the distribution means the correction to the reaction plane angle.

Let us introduce this correction explicitly and define a new angle as:

$$\psi' = \psi + \Delta\psi. \tag{18}$$

We write $\Delta\psi$ in the form:

$$\Delta\psi = \sum (A_n \cos(n\psi) + B_n \sin(n\psi)) \tag{19}$$

By requiring the vanishing of the nth Fourier moment of the new distribution, the coefficients A_n, B_n can be evaluated by the original distribution.

$$\langle\cos(n\psi')\rangle = 0 \tag{20}$$

$$= \langle\cos(n\psi + n\Delta\psi)\rangle \tag{21}$$

$$\simeq \langle \cos(n\psi) \rangle - \langle \sin(n\psi) n\Delta\psi \rangle \tag{22}$$

$$= \langle \cos(n\psi) \rangle - n\ B_n/2 \tag{23}$$

$$B_n = \frac{2}{n} \langle \cos(n\psi) \rangle \tag{24}$$

$$\langle \sin(n\psi') \rangle = 0 \tag{25}$$

$$= \langle \sin(n\psi + n\Delta\psi) \rangle \tag{26}$$

$$\simeq \langle \sin(n\psi) \rangle + \langle \cos(n\psi) n\Delta\psi \rangle \tag{27}$$

$$= \langle \sin(n\psi) \rangle + n\ A_n/2 \tag{28}$$

$$A_n = \frac{-2}{n} \langle \sin(n\psi) \rangle \tag{29}$$

So,

$$\psi' = \psi + \sum \frac{2}{n} (-\langle \sin(n\psi) \rangle \cos(n\psi) + \langle \cos(n\psi) \rangle \sin(n\psi)) \tag{30}$$

In practice, we need to implement the correction up to $n = 4$ because of the intrinsic four-fold geometric symmetry of the calorimetry.

B. Correction for the non-flatness of the reaction plane distribution

Suppose our detector is located at azimuthal angle ϕ in the lab system. Experimentally the Fourier coefficient v_1^{obs} (before correction for the reaction plane resolution) is evaluated as:

$$v_1^{obs} = \frac{\int \frac{dN}{d(\phi - \Psi_1)} \cos(\phi - \Psi_1) P(\Psi_1) d\Psi_1}{\int \frac{dN}{d(\phi - \Psi_1)} P(\Psi_1) d\Psi_1}, \tag{31}$$

where, $dN/d(\phi - \Psi_1)$ is the particle azimuthal distribution:

$$dN/d(\phi - \Psi_1) \simeq N_0(1 + 2v_1^{true} \cos(\phi - \Psi_1)), \tag{32}$$

and $P(\Psi_1)$ is the reaction plane angle distribution, which ideally should be flat, but in practice always has small anisotropy:

$$P(\Psi_1) \simeq P_0(1 + 2a_1 \cos(\Psi_1) + 2b_1 \sin(\Psi_1)). \tag{33}$$

We assume that v_1^{true}, a_1, and $b_1 \ll 1$. Then in the first order approximation

$$\begin{aligned} v_1^{obs} &= \int (1 + 2v_1^{true}\cos(\phi - \Psi_1) + 2a_1\cos(\Psi_1) + 2b_1\sin(\Psi_1))\cos(\phi - \Psi_1)d\Psi_1 \\ &= v_1^{true} + a_1\cos(\phi) + b_1\sin(\phi). \end{aligned} \tag{34}$$

Averaging over the acceptance (which is different for particles with different rapidity and transverse momentum) one gets:

$$\begin{aligned} v_1^{true} &= v_1^{obs} - (a_1\langle\cos(\phi)\rangle + b_1\langle\sin(\phi)\rangle) \\ &= v_1^{obs} - v_1^{bkgr}. \end{aligned} \tag{35}$$

This correction formula can be easily generalized for higher moment signals v_n^{true}.

The correction v_1^{bkgr} vanishes, if either Ψ_1 is flat, i.e., $a_1 = b_1 = 0$, or the acceptance of the detector is constant over full 2π azimuthal angle range (to some extend this is the case in our multiplicity flow analysis).

C. Event sample bias

In this section we discuss how the bias (with respect to the reaction plane orientation) in the event sample propagates to the results of flow analysis. We claim that at least up to the second order in a such bias the results of our analysis are not sensitive to it.

An event sample is usually defined in accordance with centrality, which in its turn is defined in accordance with PCal (TCal) E_T. Due to asymmetry in the calorimeter geometry or miscalibration such event sample can be biased. The simplest bias is just a "shift" in some direction (denoted below by Φ):

$$\frac{dN_{ev}}{d\psi_r} \propto 1 + 2A\cos(\psi_r - \Phi). \tag{36}$$

In our analysis we can never observe this effect because any non-flatness of the reaction plane distribution we attribute to the non-perfectness of the reaction plane determination. Then we introduce a new angle which eliminates the "non-flatness":

$$\psi_r' = \psi_r + \Delta\psi_r, \tag{37}$$

$$\frac{dN_{ev}}{d\psi_r'} = const = \frac{dN_{ev}}{d\psi_r}\frac{d\psi_r}{d\psi_r'}. \tag{38}$$

It gives:

$$\Delta\psi_r = 2A\sin(\psi_r - \Phi). \tag{39}$$

Taking into account the bias in the event sample the distribution of particles measured by the detector (located at azimuthal angle ϕ) will be:

$$\frac{dn}{d\psi_r} \propto \frac{dN_{ev}}{d\psi_r}(1 + 2v_1\cos(\psi_r - \phi)), \tag{40}$$

or

$$\frac{dn}{d\psi_r'} \propto 1 + 2v_1\cos(\psi_r' - \phi - \Delta\psi). \tag{41}$$

Then the observed flow signal

$$v_1' = \langle\cos(\psi_r' - \phi)\rangle = (2\pi)^{-1}\int_0^{2\pi}\cos(\psi_r' - \phi)(1 + 2v_1\cos(\psi_r' - \phi - \Delta\psi))d\psi_r' \tag{42}$$

$$v_1' = (2\pi)^{-1}\int_0^{2\pi} d\psi_r'\cos(\psi_r' - \phi)2v_1(\cos(\psi_r' - \phi)\cos(\Delta\psi) - \sin(\psi_r' - \phi)\sin(\Delta\psi)) \tag{43}$$

Expanding $\cos(\Delta\psi)$ and $\sin(\Delta\psi)$ in series and taking into account that

$$\int_0^{2\pi} d\psi_r'\cos(\psi_r' - \phi)2v_1\sin(\psi_r' - \phi)\sin(\psi_r' - \Phi) = 0 \tag{44}$$

one can see that at least up to the second order in $\Delta\psi$

$$v_1' = v_1. \tag{45}$$

D. "Blast" event bias

About 2 to 4% of all events are (sometime called "blast") events, when the entire DCII or sometimes DCIII fires. It was a common belief that such events happen randomly and has nothing to do with real interaction. However, after the close look it appears that the reason for them is certainly physics. These events are strongly correlated with PCal E_T and flow! Due to DCII blast, such events are removed from the sample of events. The correlation with flow introduces a bias in the flow analysis and has to be taken into account.

In Fig. 18 we show

a) fraction of "blast" events as a function of PCal E_T.

b) nhits_mwpc1 vs. number of reconstructed tracks. One can see that "blast" (ntrk=0) events have reasonable number of hits in mwpc.

c) fraction of "ntrk=0" events as a function of flow angle (from 4-th window – pcw4)

d) the dependence of flow signal as a function of number of identified protons in the spectrometer. From a general consideration it should be linear. Open squares – from the entire sample, filled circles – from the sample with $ntrk > 0$ (without "blast" events).

E. Occupancy correction

It is known that the efficiency of the reconstruction of two tracks close in DC2 and/or DC3 (with relative separation less than 1 cm and 2 cm, respectively) is relatively low. The number of lost tracks in this case is proportional to the total number of tracks in the spectrometer, or to the spectrometer occupancy.

The correction for these lost tracks is called "the occupancy correction". The mean number of tracks in the spectrometer depends on the centrality and (what is important for flow study) also on the reaction plane angle. The occupancy is higher for the events with the reaction plane orientation into the spectrometer, and consequently the number of lost tracks is also higher. The negligence of the effect results in the underestimate of the flow signal.

We start with a simple estimate of a possible bias due to the efficiency dependence on occupancy. The occupancy of a 2 cm bin in DC2 is approximately 0.4. The variation in the occupancy due to flow could be as high as 20%. Then one can write

$$\overline{n} = 0.4(1 - 2 \cdot 0.05 \cos(\psi)) \tag{46}$$

The correction for the lost tracks will be

$$\exp(\overline{n}) \approx 1 + 0.4(1 - 2 \cdot 0.05 \cos(\psi)) \propto 1 + 2 \cdot 0.05/1.4 \cos(\psi) \approx 1 + 2 \cdot 0.03 \cos(\psi) \tag{47}$$

From this it is clear that the maximal possible bias in v_1 due to occupancy is about 3%.

We apply the prescription of occupancy correction described in [[7]] by assigning extra weight equal to 1.5 to any track each time it has another track found in the vicinity of minimum separation (DC2: 1 cm, DC3: 2 cm).

In Fig. 19, we show the dependences of the occupancy weight of tracks identified as proton on transverse momentum p_t , centrality of events, orientation of the reaction plane and rapidity region. Pion tracks show similar dependence with less extra weight than one.

F. Particle Identification

Before making any particle identification we apply the following selection criteria to the tracks found in the spectrometer:

1. "software" collimator geometrical acceptance cut:
   `(px/pz.lt.-0.140 .and. px/pz.gt.0.007`
   `.and. py/pz.lt.-0.008 .and. py/pz.gt.0.010)`,
2. p_y information is required (vertical information from at least one of drift chambers)
3. Y position matching in DCII, DCIII, and TOFU:
   `((abs(py/pz*5380000.-dc2y).lt.6000.) .or.`
   `(abs(py/pz*11600000.-dc3y).lt.4000.))) .and.`
   `(abs(py/pz*12290000.-y).lt.30000)`,
4. TOFU pulse height cut:
   `(ph.gt.0.85 .and. ph.lt.(1.3+0.025*(t-path)))`,
5. no other tracks pointing to the same tofu slot,
6. track does not go through drift chamber dead regions,
7. TOFU slots considered as "non-reliable" are removed from the analysis.
8. p_x cut (`px.lt.0.` (Avoid the albedo source located at the collimator edge ?).

Particle identification is made in accordance to the value of calculated mass squared m^2 for good tracks. In the experiment, there are three measurables related to a particle:

momentum (p), time of flight (TOF), and flight path length (L). From them, we calculate the mass squared as

$$m^2 = p^2(\frac{1}{\beta^2} - 1) = p^2((\frac{TOF}{L})^2 - 1), \tag{48}$$

where β is the particle velocity.

According to [8] the resolution in reconstructed mass squared consists of two parts, the momentum resolution of the tracking system and the time resolution of the time of flight system. This is true under the assumption of the constantness of time of flight resolution. In this case the mass squared resolution could be written as a function of momentum.

$$\begin{aligned}\sigma^2_{m^2} &= 4m_0^2(\frac{\sigma_p}{p})^2 + \frac{4p^4}{\beta^2}(\frac{\sigma_{TOF}}{L})^2 \\ &= c_1^2(4m_0^2p^2) + c_2^2(4m_0^2(1+\frac{m_0^2}{p^2})) + c_3^2(4p^2(m_0^2+p^2)),\end{aligned} \tag{49}$$

where

$$\begin{aligned}\sigma^2_{m^2} &: \text{the resolution of reconstructed mass squared} \\ m_0 &: \text{assumed known mass of the particle} \\ p &: \text{measured momentum of the particle} \\ \sigma_p &: \text{momentum resolution} \\ \sigma_{TOF} &: \text{time of flight resolution} \\ L &: \text{flight path length} \\ c1, c2, c3 &: \text{Determined coefficients}\end{aligned}$$

c1,c2,c3 are the coefficients representing angular resolution, multiple scattering and time of flight resolution.

Fit of the m^2 distribution around the peak in each momentum slice by Gaussian provides the mean value of m_0^2 and the width $\sigma^2_{m^2}$ as a function of momentum p. The width is then fitted with the formula (49). The obtained values of c_1, c_2, c_3 for proton and charged pions are shown in the Table I for different magnetic field polarities.

Field	A Field		B Field	
particle	p	π	p	π
c1	0.0079	0.0000042	0.0073	0.0000042
c2	0.0371	0.00413	0.0354	0.00413
c3	0.00206	0.00177	0.00186	0.00177

TABLE I. Parameters of particle identification in 93 data

The particle identification is performed by selecting hits within some range proportional σ_{m^2} around the mean value of m^2 in each momentum p slice. In the order to get clean identification and cut out low momentum contamination of e^+, e^-, and misidentified tracks from charged pion samples, we impose a stringent cut of $1.5\,\sigma$ around m_0^2. Even though the fitted mean m^2 fluctuate around m_0^2, we use m_0^2 in all momentum range in making the particle identification cut. In order to avoid the possible mixing of particles in high momentum region, we require one additional highest momentum cut to clean the possible misidentification.

`(p.lt.11)` for proton to prevent deutron contamination, and

`(p.lt.6)` for pion to prevent kaon or proton. The dependence of the flow signal on this cut is under study now.

We demonstrate our particle identification in $p - m^2$ and $1/p - TOF$ plots in Fig. 17.

94 94 94 94 94 94 94 94 94 94 94 94 94 94 94 94 94 94 94 94 94 94

Mark Pollack provides the PID for 94 data as a reference:

To extract the coefficients from the data a plot of m^2 vs p was made using the 1994 data. Only global "event-quality" cuts were applied. This plot was sliced into several momentum windows. For each window the m^2 distribution was fit to extract the mass width of pions, kaons, protons and deuterons. A single Gaussian was used for pions and protons, while for kaons and deuterons it was necessary to introduce a background function in addition.

The width as a function of momentum was then fit with formula (Eq 49). The obtained values of c_1, c_2, c_3 are shown in Table II and a plot of the data along with the fit are shown in Figurexxx. Except for some deviations for the pions, the fit is excellent and show that the spectrometer response is accurately modeled by Eq. 49 for all particle species.

particle	c1	c2	c3	chi2 ndof	sigtof (ps)
pion	$0.0024(fixed)$	$0.0289(fixed)$	0.002181 ± 0.000006	11.4	90
kaon	$0.0024(fixed)$	0.0277 ± 0.00133	0.001846 ± 0.00004	0.4	76
proton	$0.0024(fixed)$	0.0298 ± 0.00011	0.002177 ± 0.00001	0.18	90
deuteron	$0.0024(fixed)$	0.0273 ± 0.00043	0.001945 ± 0.00005	0.04	80

TABLE II. Parameters of particle identification in 94 data

Some comments should be made concerning the selection of variables that were held fixed during the fit. A free fit to the data points did not give identical values for all particles. The angular resolution term was similar for the protons and deuterons while multiple scattering term was similar for the kaons, protons and deuterons. The time of flight resolution was similar for the pions, kaons, and protons. See Table III.

particle	c1	c2	c3	chi2 ndof
pion	0.0853 ± 0.002135	-0.0456 ± 0.0032	0.002020 ± 0.000006	2.0
kaon	0.0 ± 0.0042	0.0279 ± 0.00132	0.001854 ± 0.00004	0.4
proton	0.0044 ± 0.0020	0.0287 ± 0.00018	0.002131 ± 0.00001	0.14
deuteron	0.0044 ± 0.00040	0.0246 ± 0.00086	0.001288 ± 0.00023	0.03

TABLE III. Parameters of particle identification in 94 data

(get rid of strange errors and chi2/ndof - why so small..) The deuterons show a significant deviation from the expected time resolution. ($0.002 * 1000 * 41.12 = 82$ ps and the deuteron value is 53 ps) There is only some sensitivity to c1 for the deuteron fit. The separation of the momentum resolution into c1 and c2 for the pions is particularly poor, giving a negative value for c2. Performing the deuteron fit again but fixing the value of c1 to its estimated value of 0.0024 the time resolution became 0.001945. ([9]).

Fixing c1 for the other fits yielded the following results shown in Table IV

particle	c1	c2	c3	chi2 ndof
pion	$0.0024(fixed)$	0.0869 ± 0.0032	0.002115 ± 0.000003	2.8
kaon	$0.0024(fixed)$	0.0277 ± 0.00133	0.001846 ± 0.00004	0.4
proton	$0.0024(fixed)$	0.0298 ± 0.00011	0.002177 ± 0.00001	0.18
deuteron	$0.0024(fixed)$	0.0273 ± 0.00043	0.001945 ± 0.00005	0.04

TABLE IV. Parameters of particle identification in 94 data

The only value that does not agree with the others is c2 for the pions. Fixing it to 0.289 yields the final table and plots. There is a visible difference in changing c2 for the pions. The low momentum pions needs to be looked at again do see if the bin size is biasing the fit of with mass width toward higher values. For particle identification purposes the different value of c2 can be used as well as taking the average value of the data for the particle masses.

When further cuts are applied to the data, such as tofu pulse hight, y-matching between the drift chamber and tofu, vertex chamber matching, etc., the pid plots should be revisited to see if there are any noticeable changes.

94 94 94 94 94 94 94 94 94 94 94 94 94 94 94 94 94 94 94 94 94 94

FIGURE CAPTIONS

1. (a) Triple differential distribution of protons (rapidity bin $3.0 < y < 3.1$) before correction for the reaction plane resolution. (b) The same for π^+.

2. The transverse momentum dependence of the first moment (v_1) of proton azimuthal distribution for different particle rapidities and centralities of the collision.

3. The same as Fig. 2 for positive pions.

4. The same as Fig. 2 for negative pions.

5. Mean projection of the particles transverse momentum on the reaction plane ($\langle p_x \rangle$) as a function of rapidity. The results of [2] are also shown for comparison at the mid-rapidity region.

6. Transverse velocity β_x of the thermal (proton) source for different proton rapidities and centralities of the collision.

7. The dependence of inverse (Boltzmann) slope parameter (T_B) of proton distribution as a function of azimuthal angle.

8. v_2 of proton distribution as a function of rapidity for different centralities.

9. v_3 of proton distribution as a function of rapidity for different centralities.

10. v_2 of π^+ distribution as a function of rapidity for different centralities.

11. v_3 of π^+ distribution as a function of rapidity for different centralities.

12. v_2 of π^- distribution as a function of rapidity for different centralities.

13. v_3 of π^- distribution as a function of rapidity for different centralities.

14. The behaviour of v_1 corresponding to the distributions (9,10).

15. The fitting of v_1 corresponding to the distributions (9(dash),10(dot)).

16. The fit parameters for the distributions (9,10).

17. (a) Particle identification on $1/p$ *vs time-of-flight* plot. (b) Particle identification on p *vs* m^2 plot.

18. Study of Blast events(details see the text).

19. The dependence of the mean weight of identified proton on p_t, centrality (PCal E_T), the reaction plane orientation (cos(PCW4)) and the particle rapidity.

[1] E877 Collaboration, J. Barrette *et al.*, Phys. Rev. Lett. **70**, 2996(1993).

[2] E877 Collaboration, J. Barrette *et al.*, "Energy and Charged Particle Transverse Flow ...", in preparation;
E877 Note #PITT-...95 "Charged Particle Directed Transverse Flow in Au+Au Collisions at 10.8 A GeV/c";
T. Hemmick for the E877 Collaboration, talk at QM '96.

[3] E877 Collaboration, J. Barrette *et al.*, "Proton and Pion Distributions in Au-Au ...", in preparation;
R. Lacasse for the E877 Collaboration, talk at QM '96.

[4] S. Voloshin and Y. Zhang, Z. Phys. C **70**, 665 (1996); *hep-ph/9407282* (July 1994).

[5] RQMD 2.3.

[6] E877 Note ???? – tracking efficiency and occupancy correction

[7] S. Voloshin, E877 Note # HD-96/08/15 and E877 Note # HD-96/08/27.

[8] K. Shigaki, Ph.D. Dissertation

[9] Dariusz Miskowiec, private communication

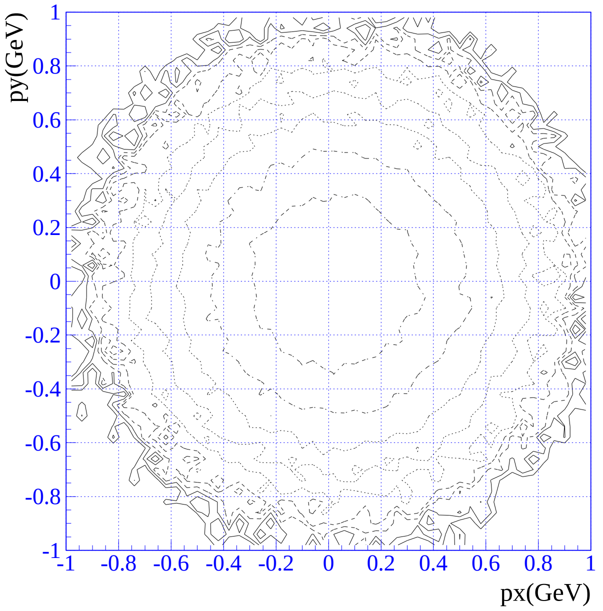

(a)

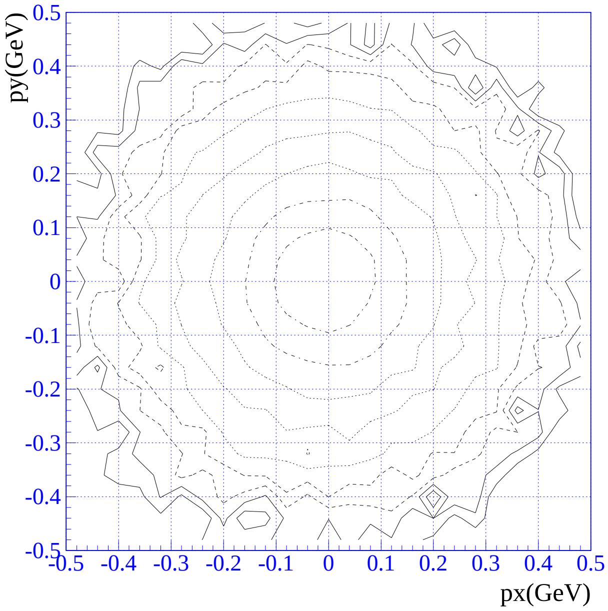

(b)

FIG. 1. Triple differential distribution of (a) protons and (b) π^+ (rapidity bin $3.0 < y < 3.1$) before correction for the reaction plane resolution.

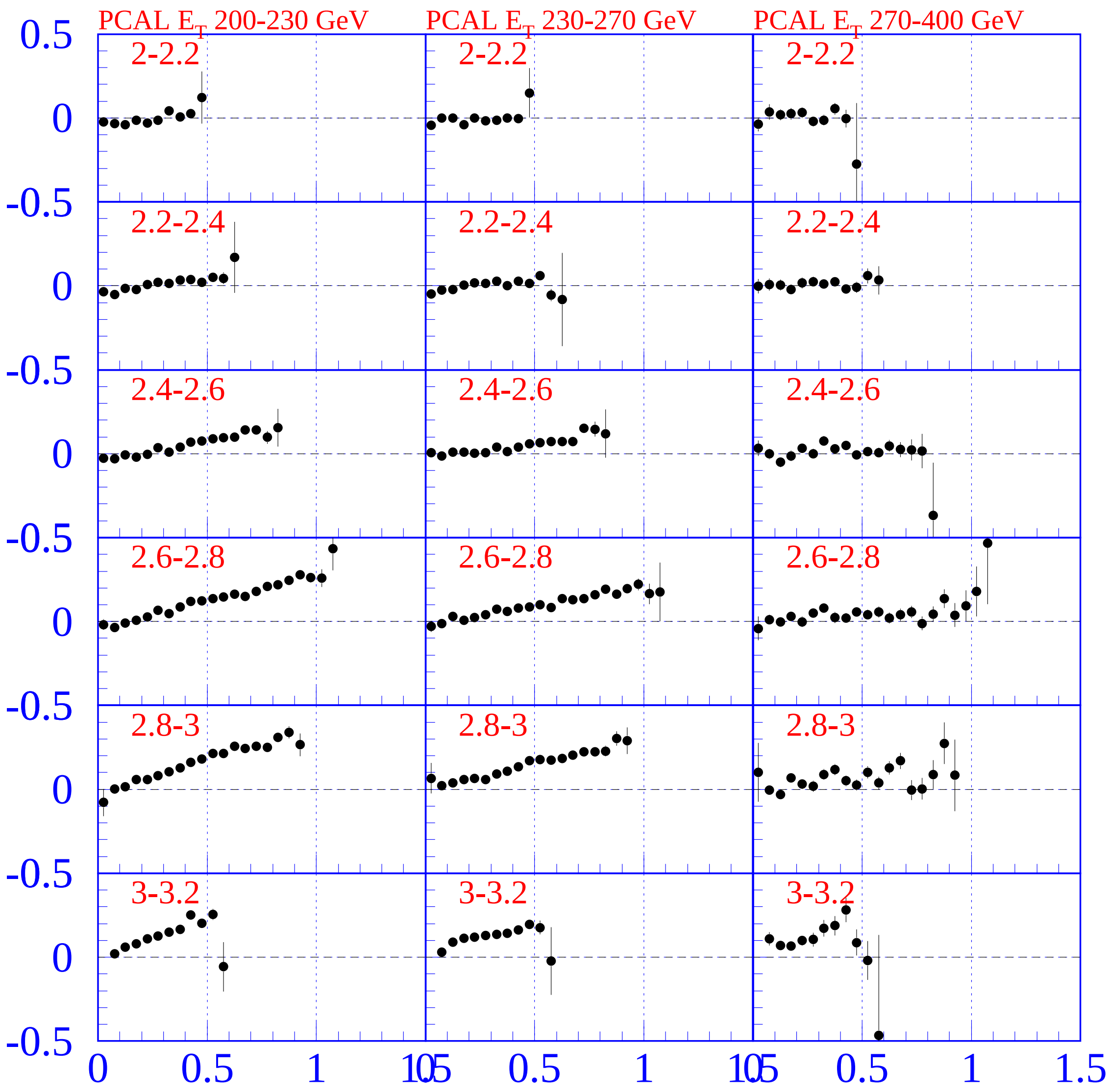

FIG. 2. The transverse momentum dependence of the first moment (v_1) of proton azimuthal distribution for different rapidities and centralities of the collision.

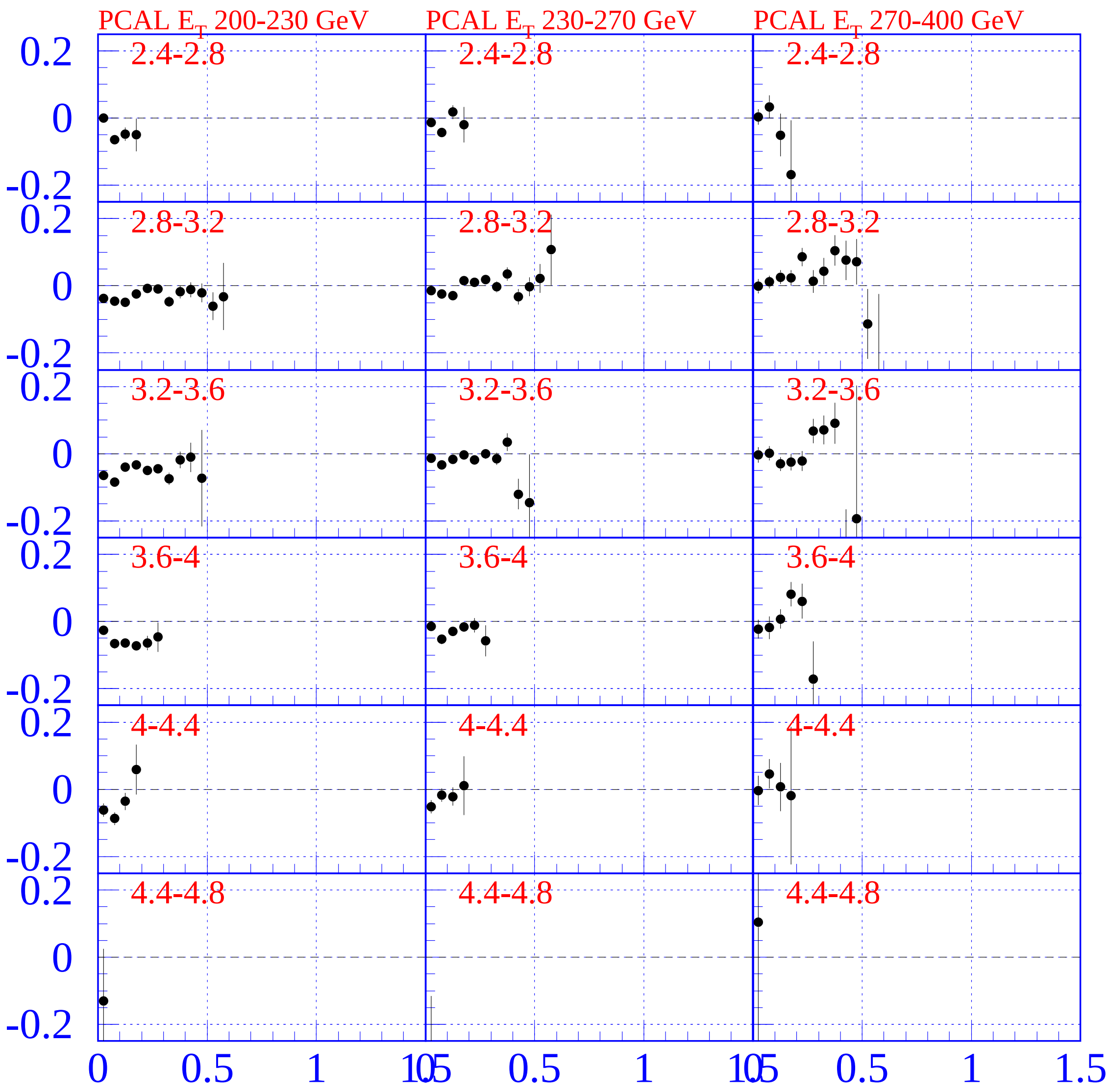

FIG. 3. The transverse momentum dependence of the first moment (v_1) of π^+ azimuthal distribution for different rapidities and centralities of the collision.

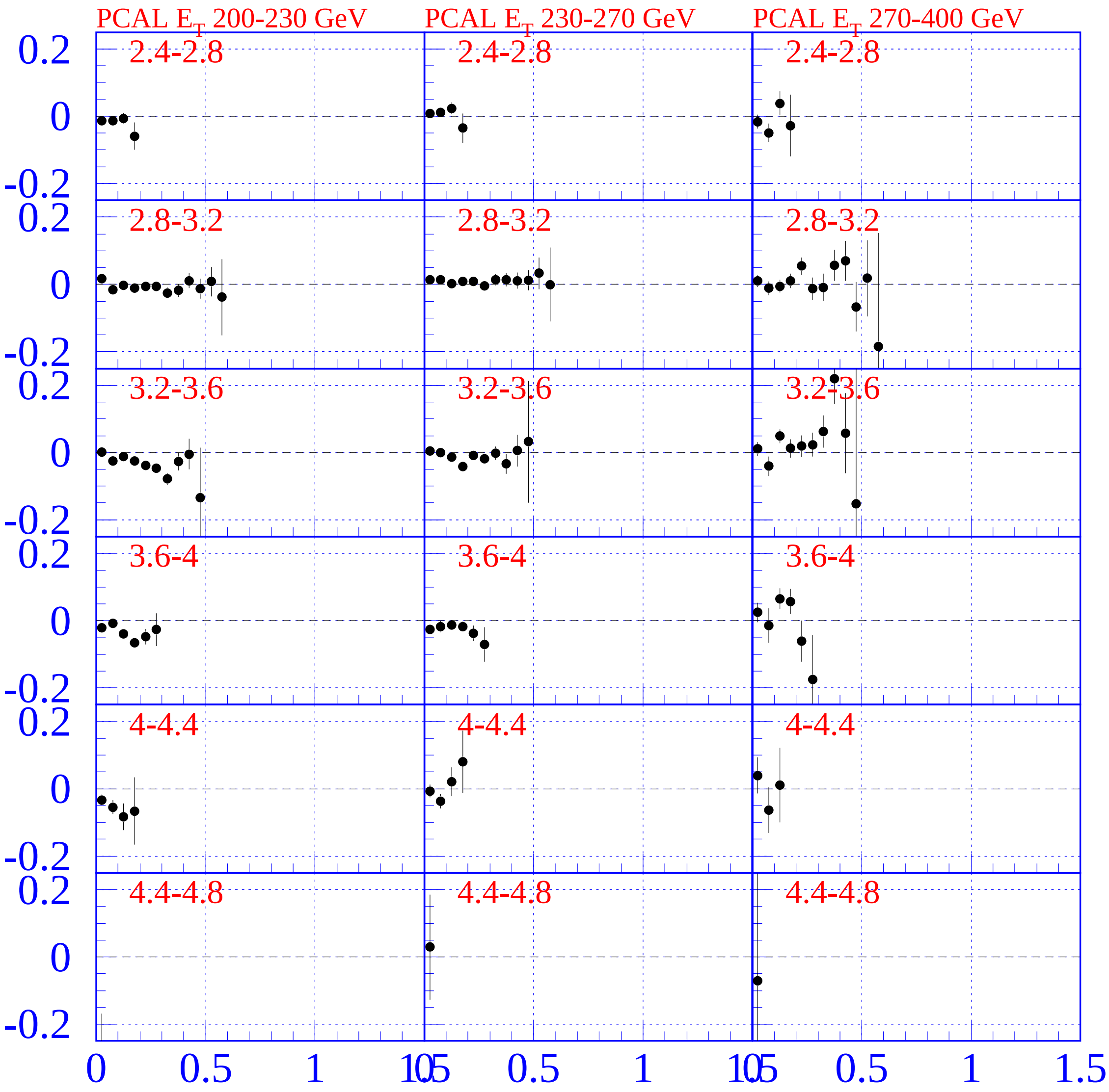

FIG. 4. The transverse momentum dependence of the first moment (v_1) of π^- azimuthal distribution for different rapidities and centralities of the collision.

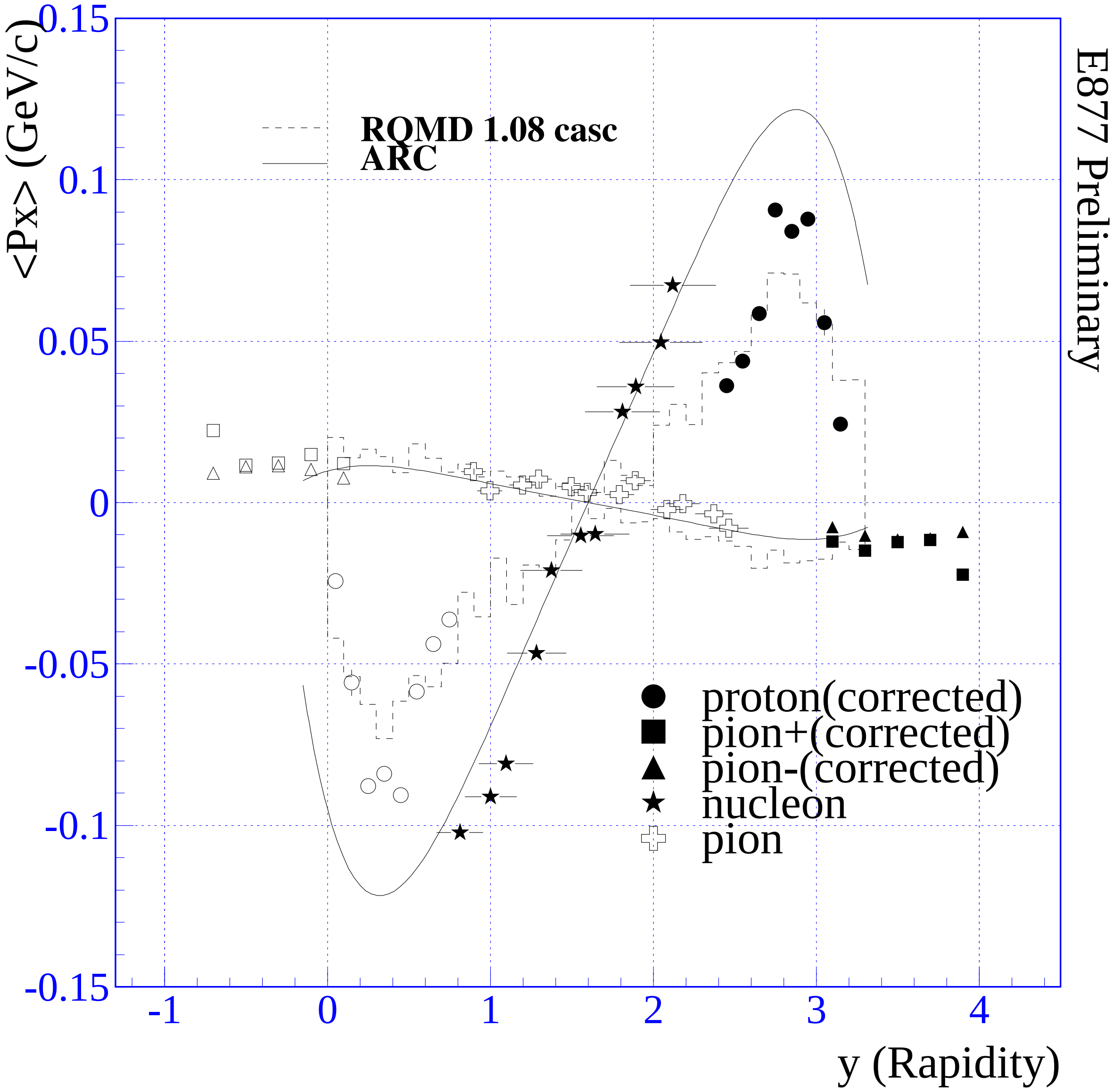

FIG. 5. Mean transverse momentum projected on the reaction plane $\langle p_x \rangle$

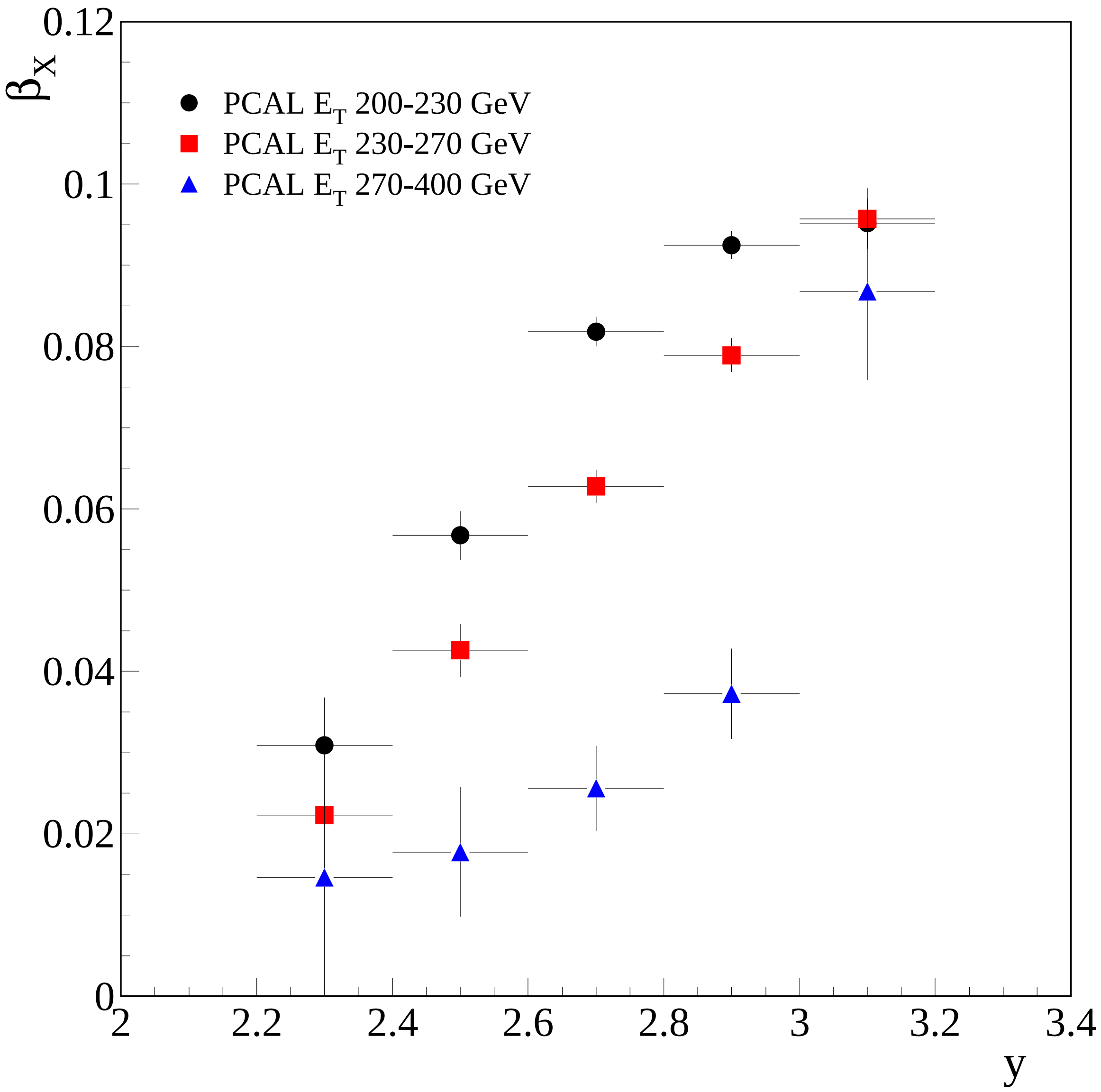

FIG. 6. Transverse velocity β_x of the thermal source model for proton in different rapidities and centralities

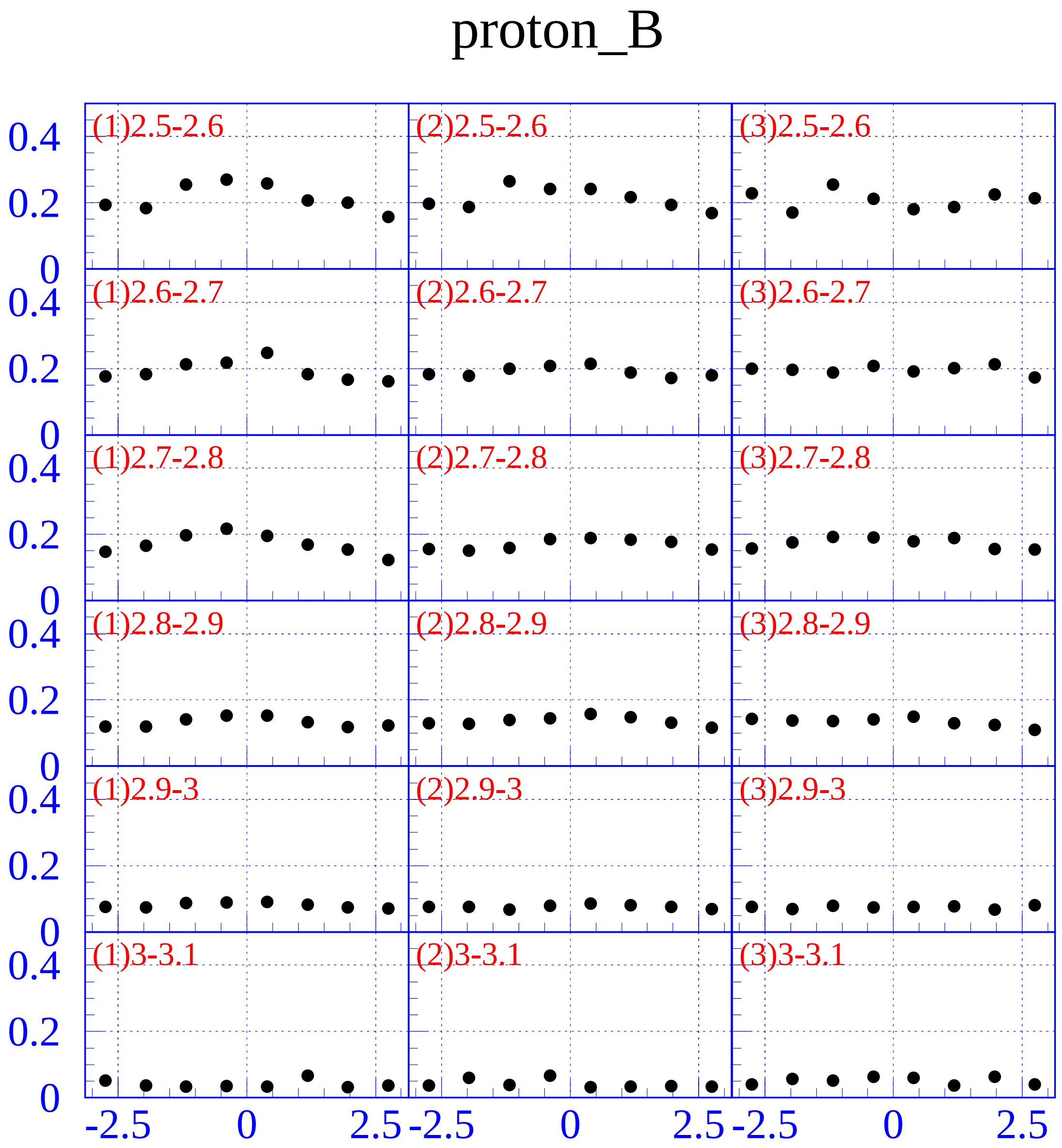

FIG. 7. The dependence of inverse (Boltzmann) slope parameter (T_B) of proton distribution as a function of azimuthal angle.

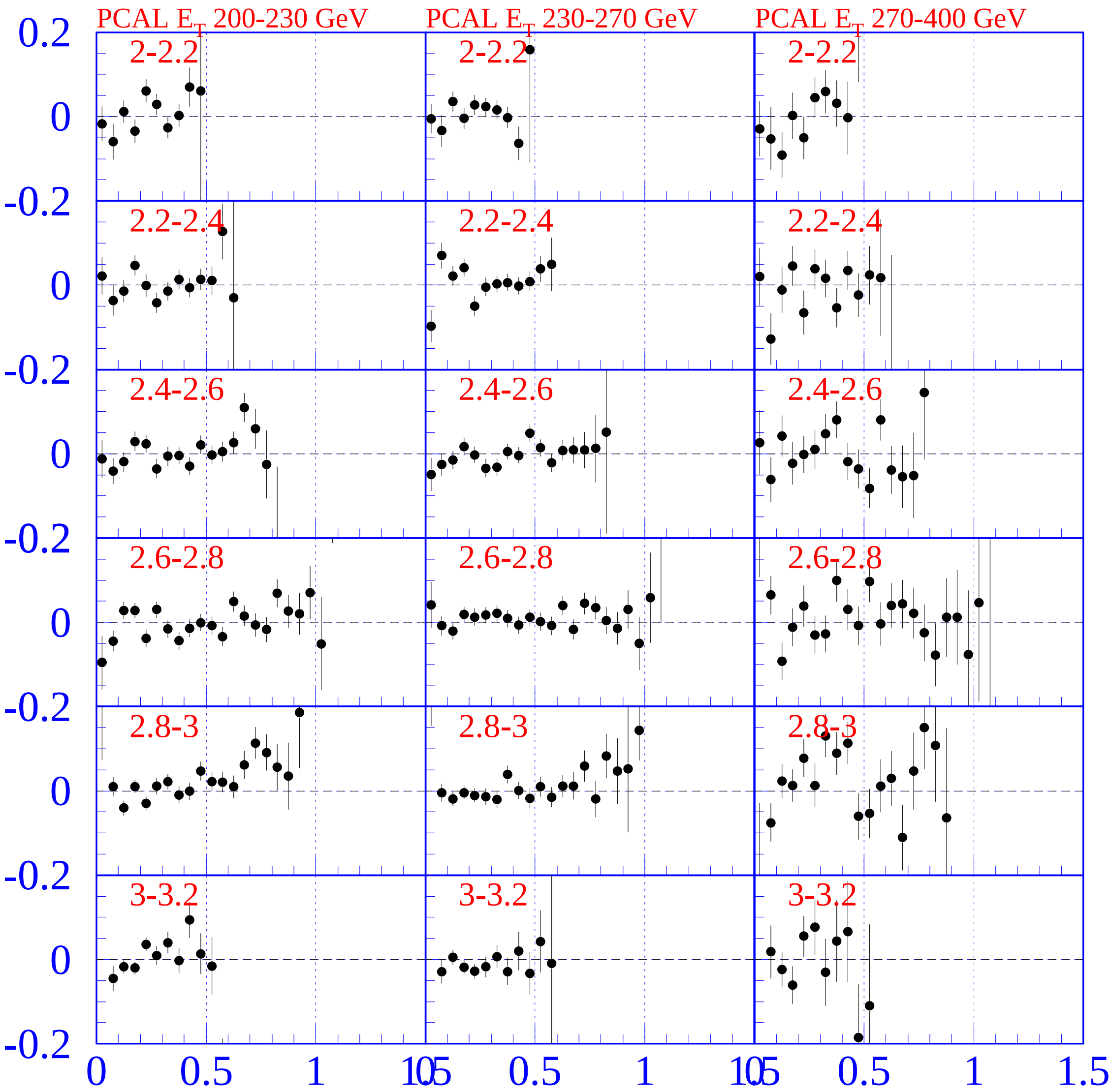

FIG. 8. The transverse momentum dependence of the second moment (v_2) of proton azimuthal distribution for different proton rapidities and centralities of the collision.

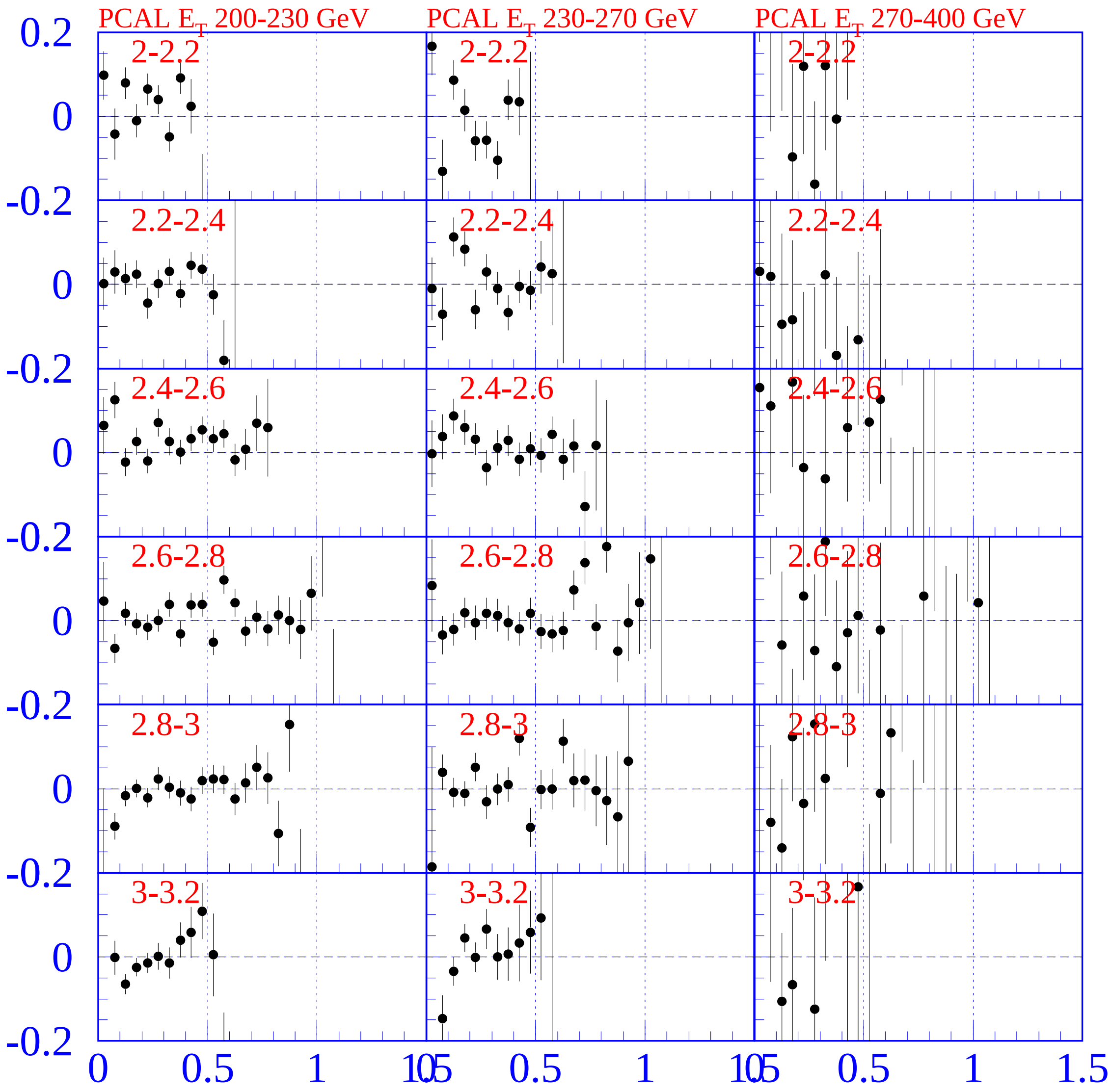

FIG. 9. The transverse momentum dependence of the third moment (v_3) of proton azimuthal distribution for different proton rapidities and centralities of the collision.

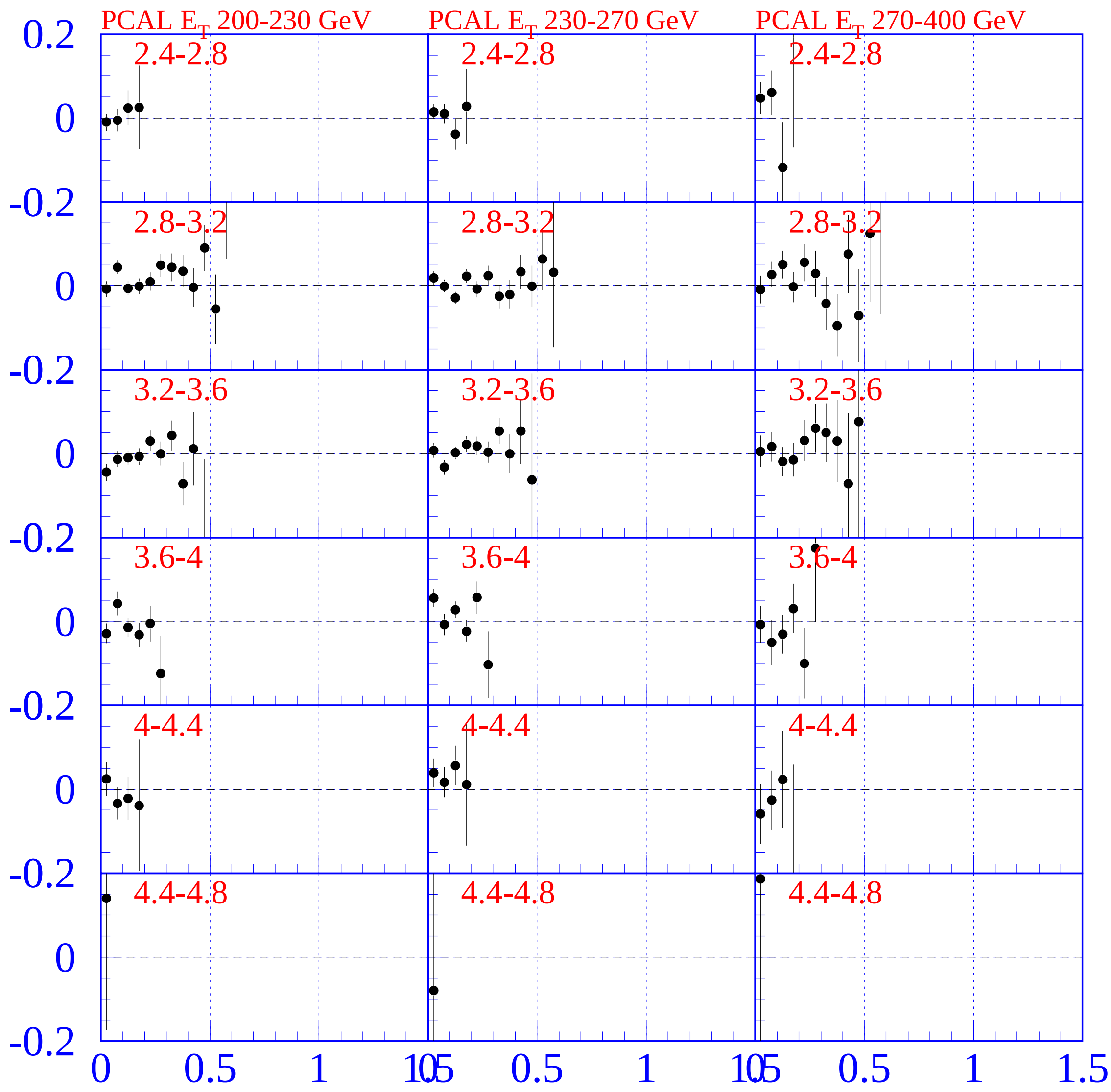

FIG. 10. The transverse momentum dependence of the second moment (v_2) of proton azimuthal distribution for different π^+ rapidities and centralities of the collision.

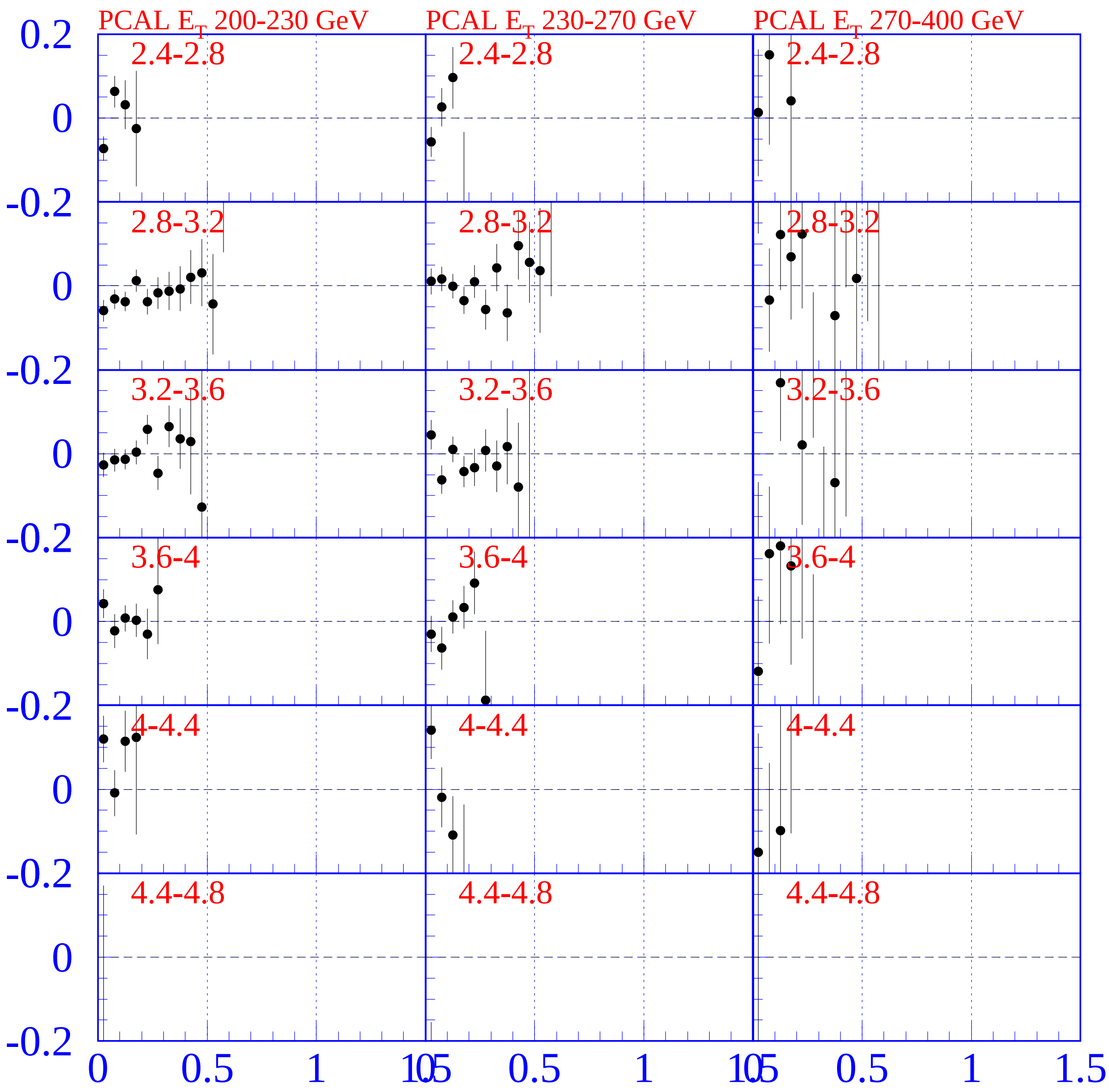

FIG. 11. The transverse momentum dependence of the third moment (v_3) of π^+ azimuthal distribution for different proton rapidities and centralities of the collision.

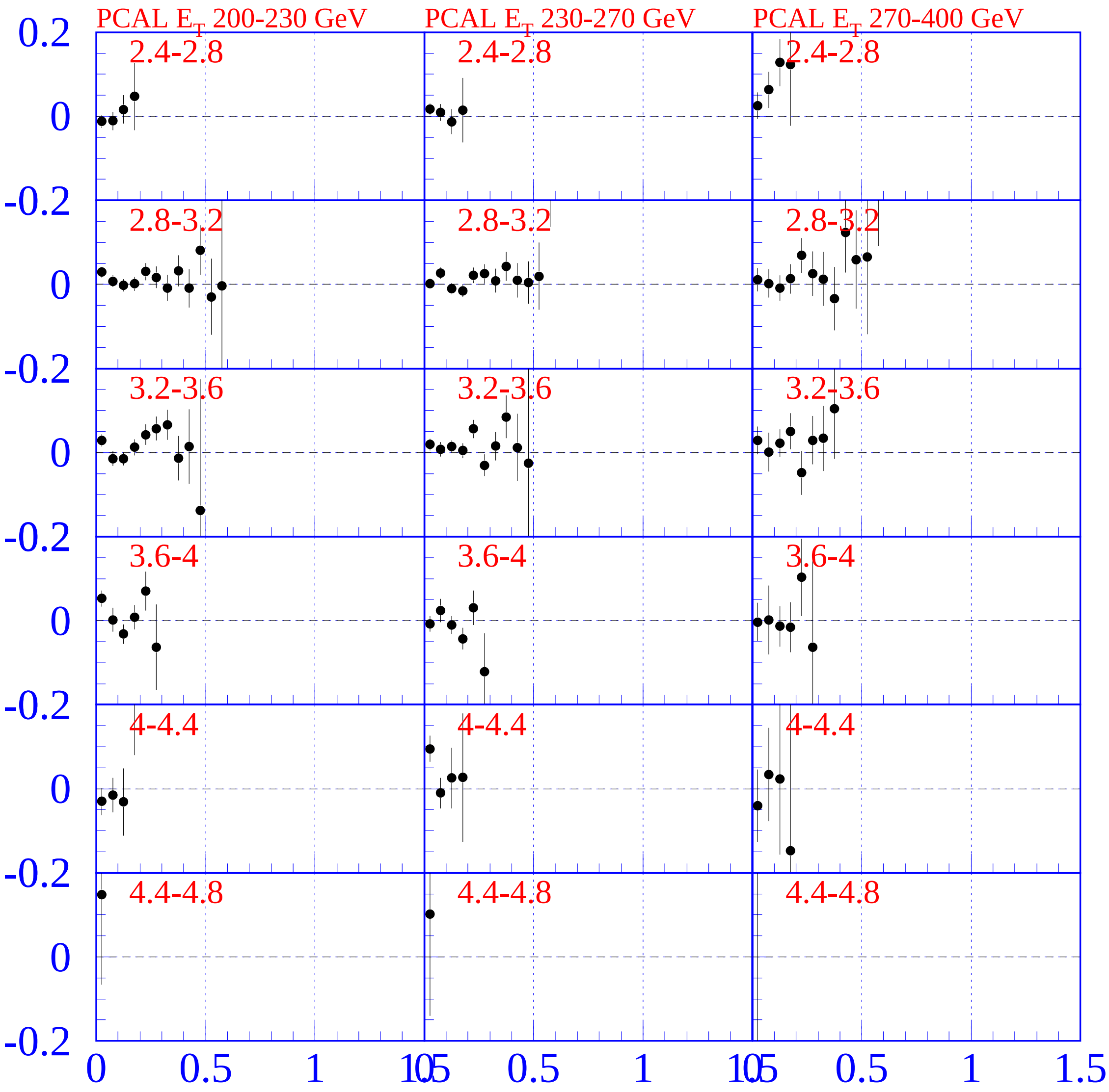

FIG. 12. The transverse momentum dependence of the second moment (v_2) of proton azimuthal distribution for different π^- rapidities and centralities of the collision.

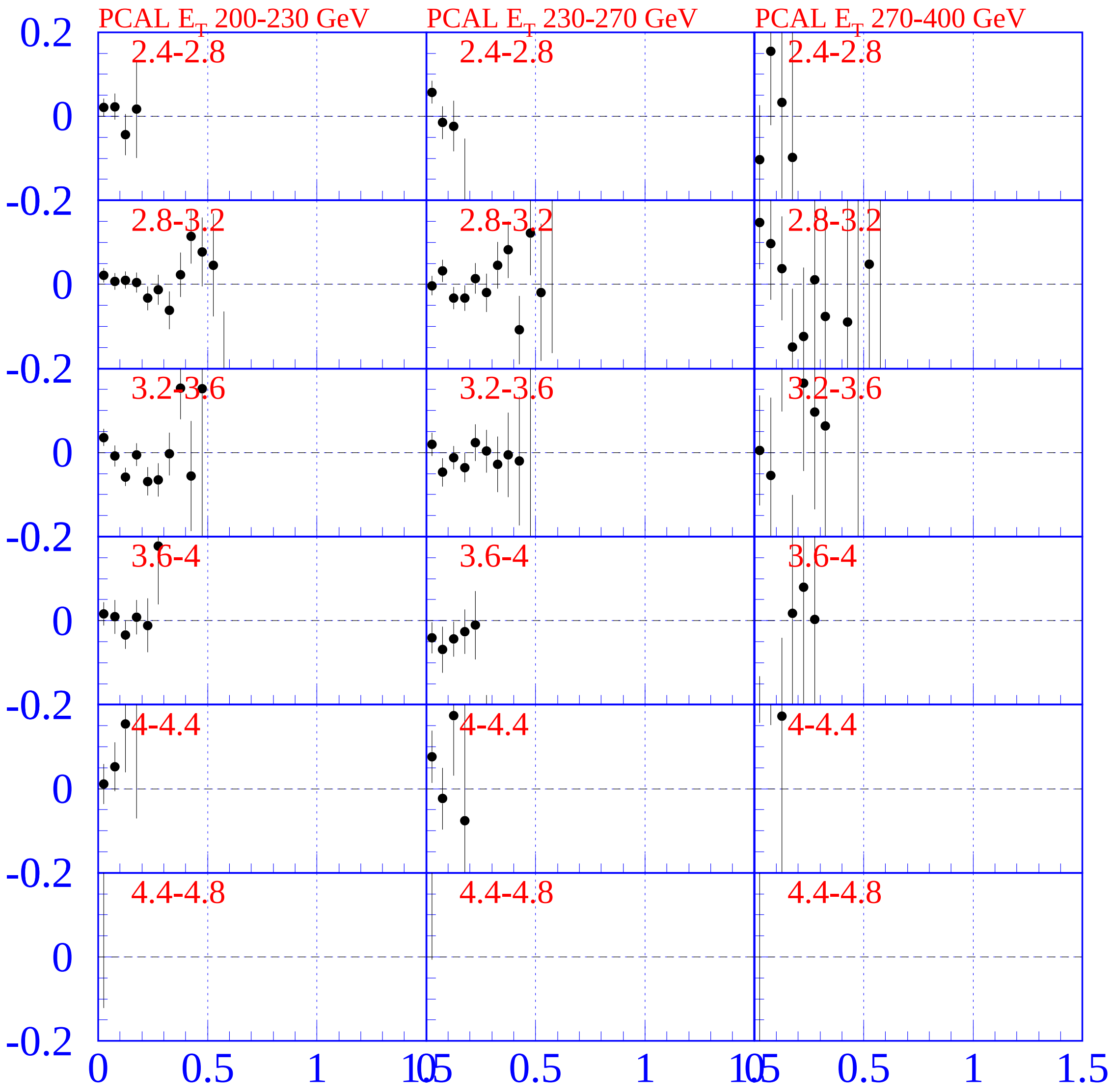

FIG. 13. The transverse momentum dependence of the third moment (v_3) of π^- azimuthal distribution for different proton rapidities and centralities of the collision.

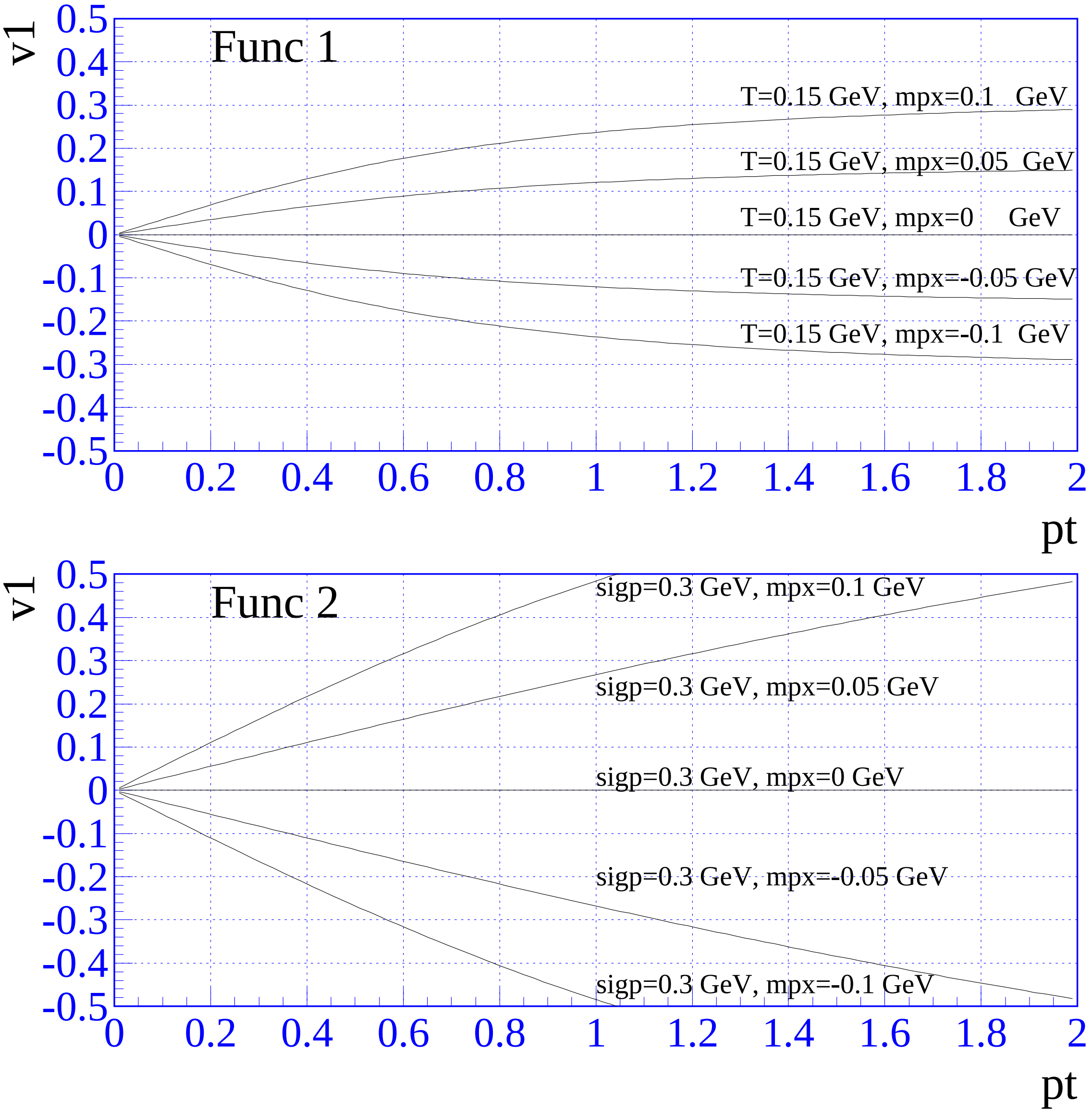

FIG. 14. The behaviour of v_1 corresponding to the distributions (9,10).

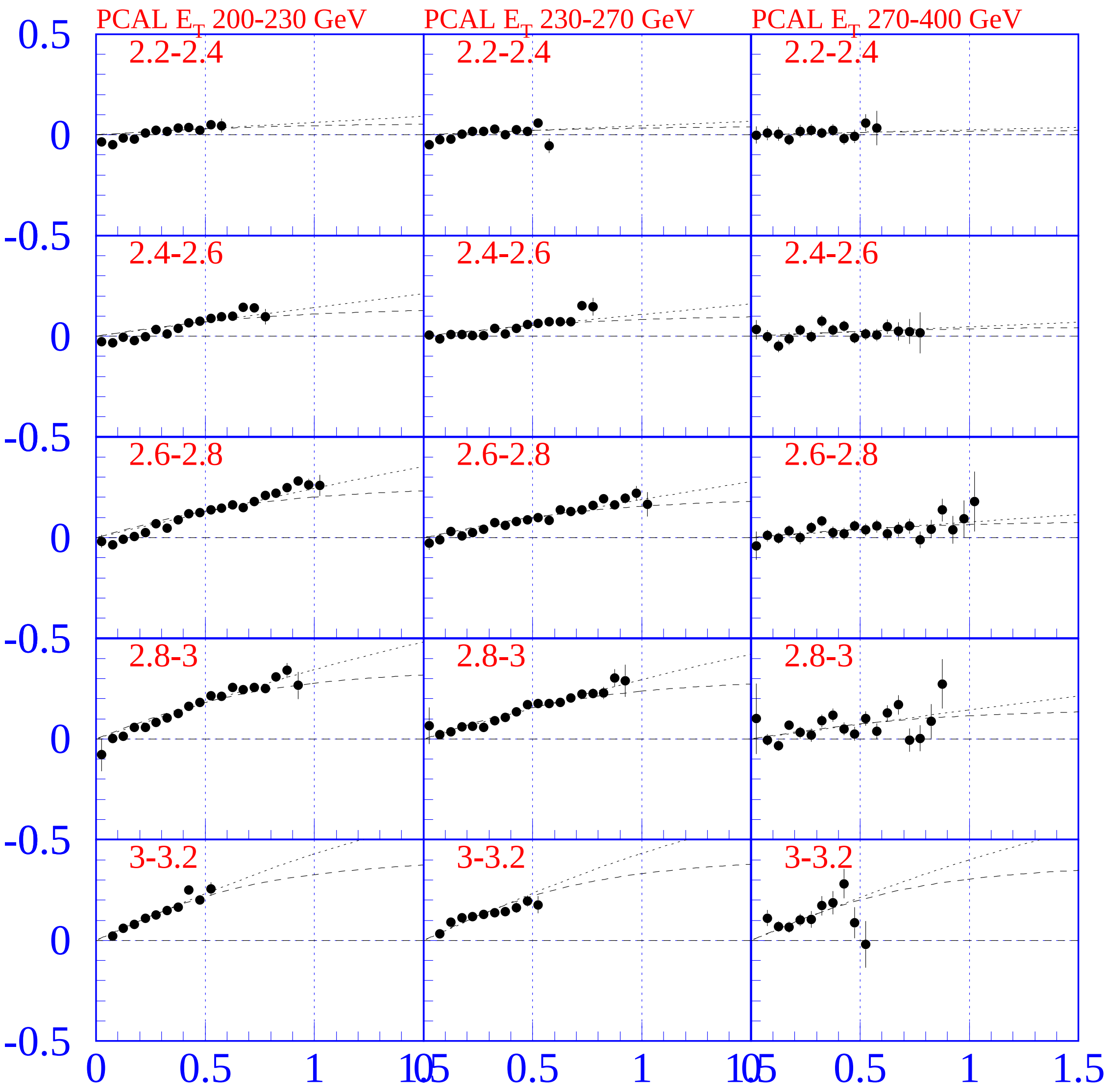

FIG. 15. The fitting of v_1 corresponding to the distributions (9(dash),10(dot)).

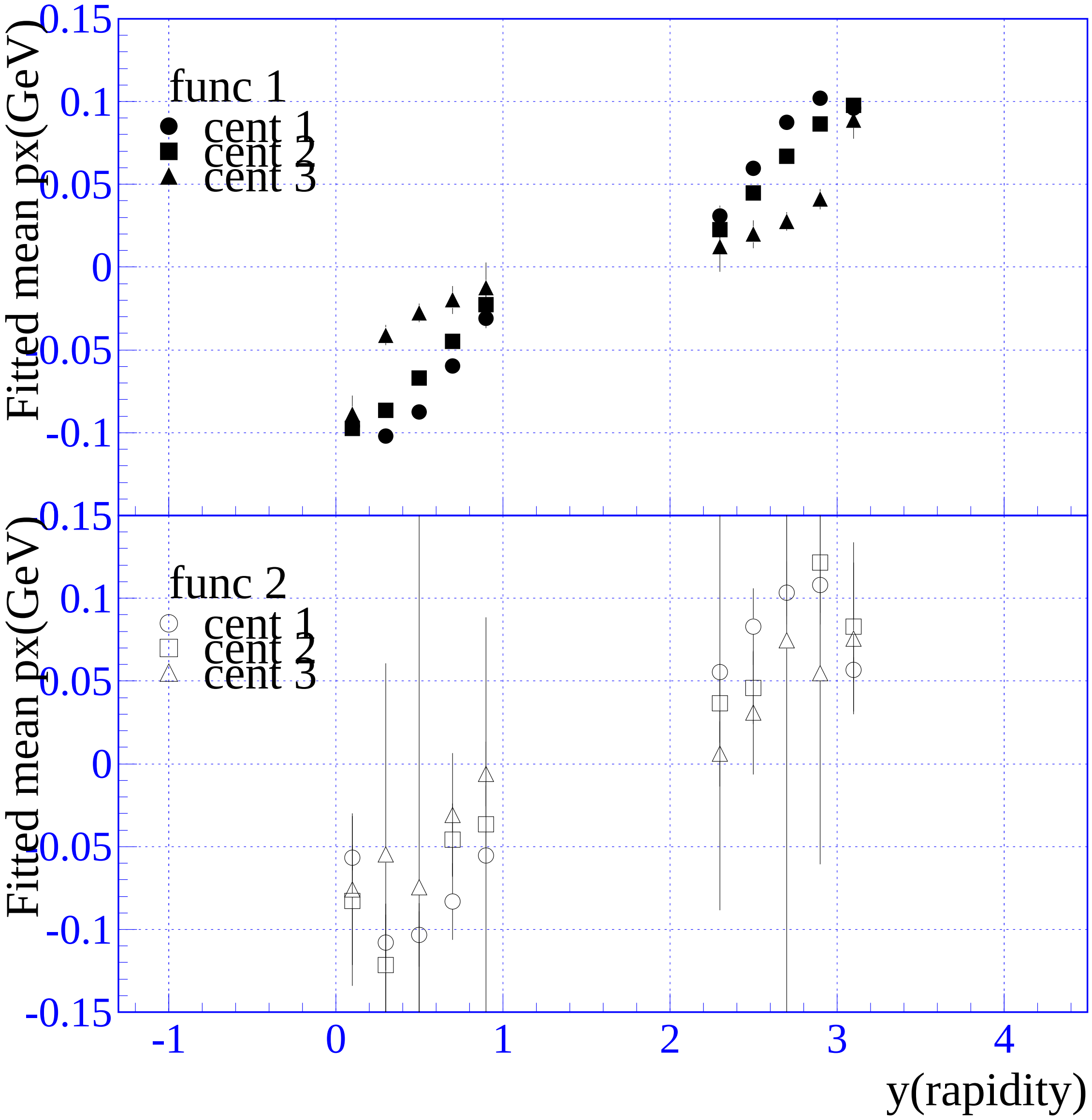

FIG. 16. The fit parameters for the distributions (9,10).

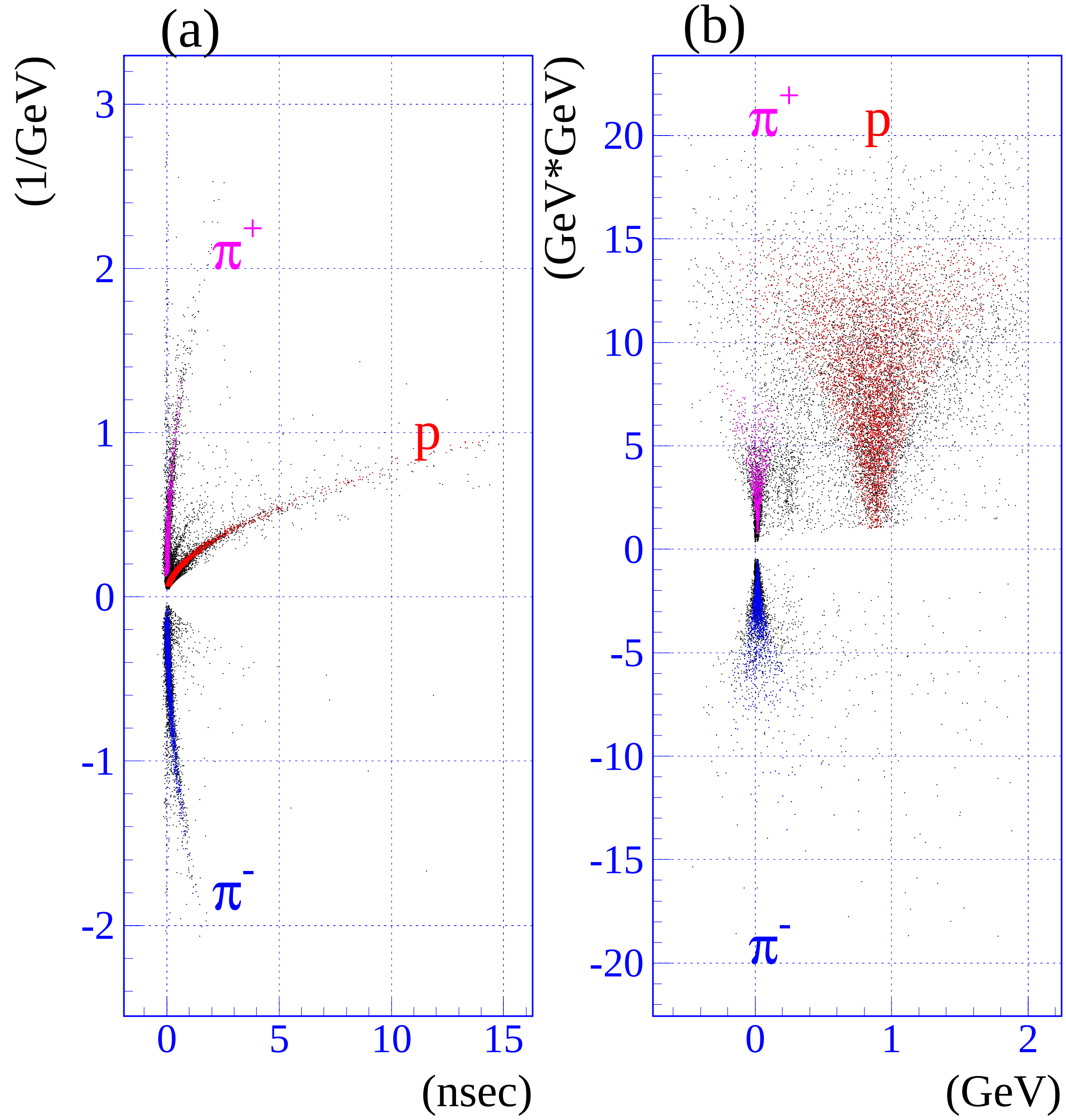

FIG. 17. (a) Particle identification on $1/p$ *vs time-of-flight* plot.
(b) Particle identification on p *vs* m^2 plot.

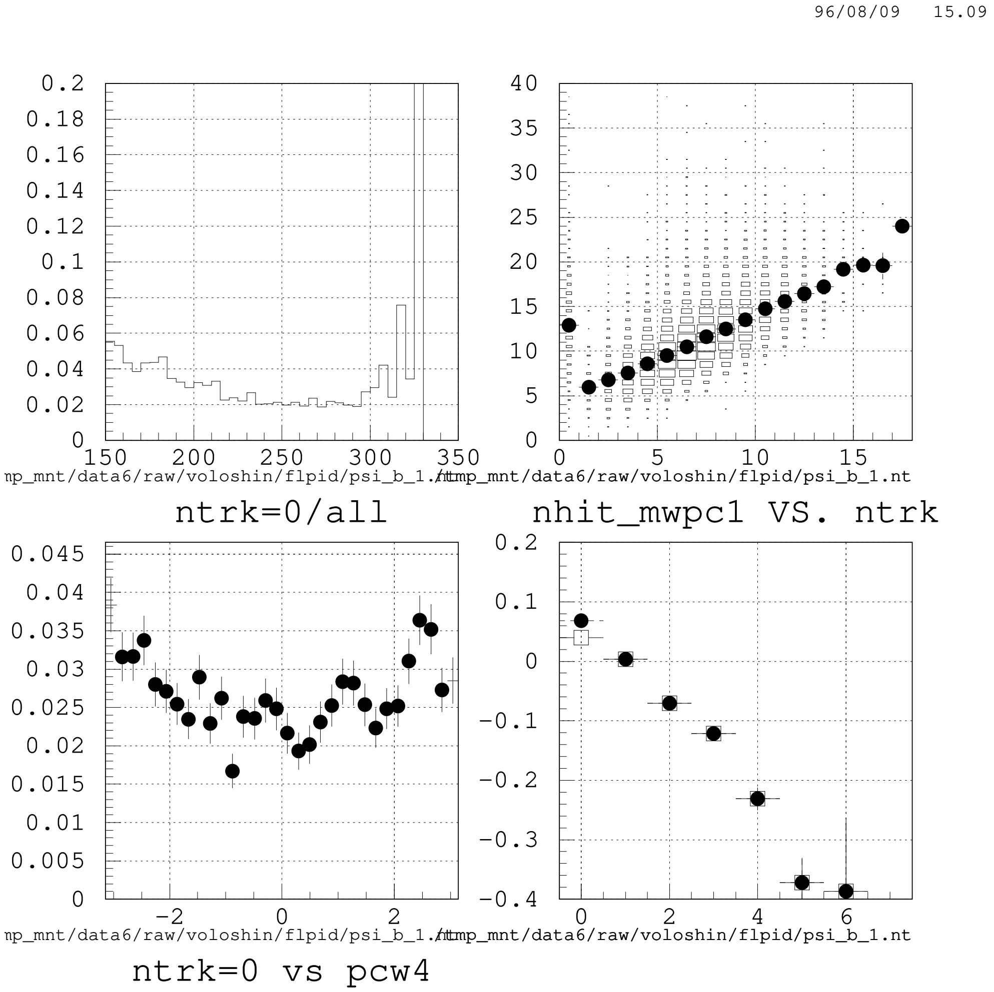

FIG. 18. The study of blast event(details see the text)

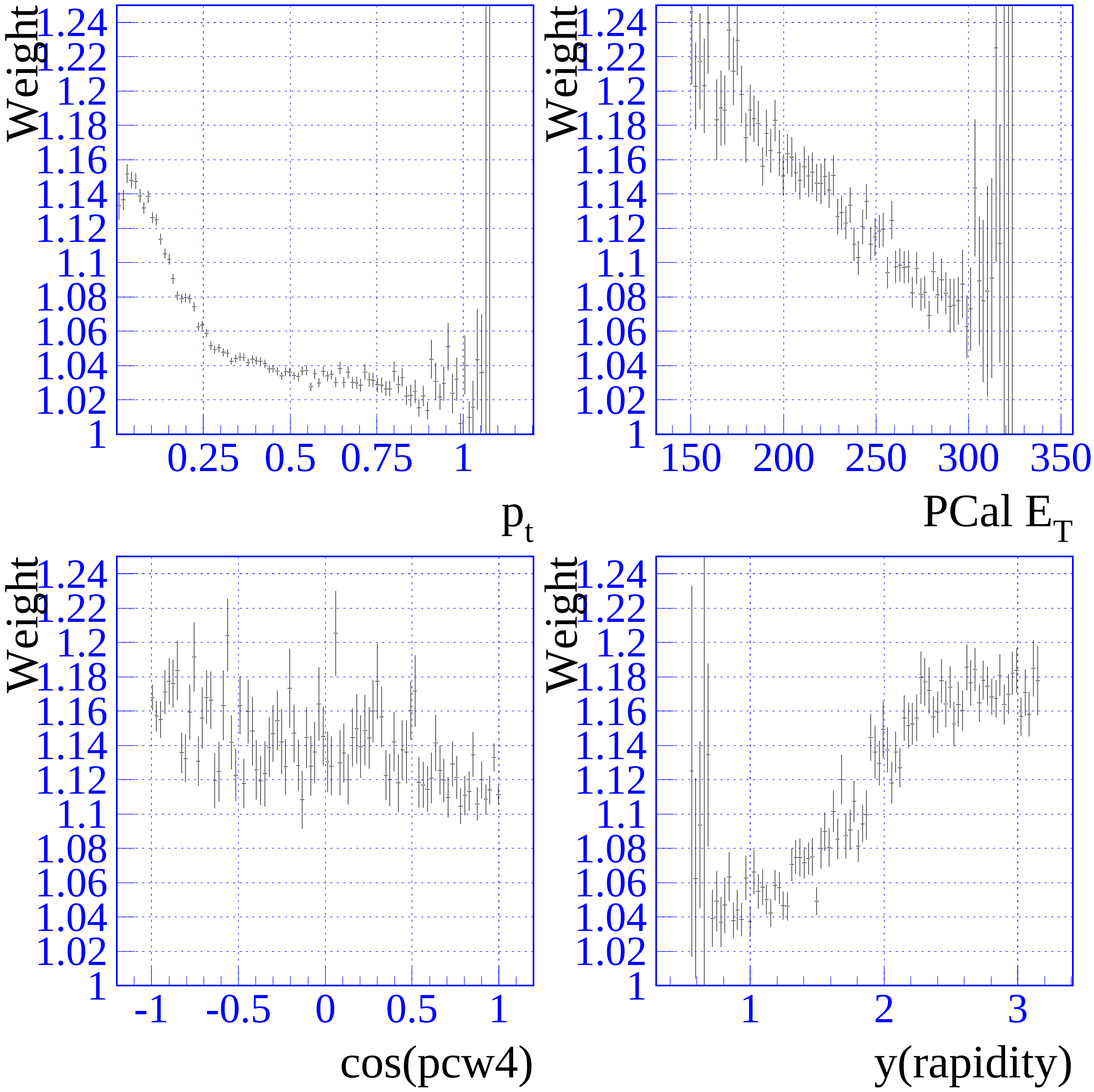

FIG. 19. The dependence of the mean weight of identified proton on p_t, centrality (PCal E_T), the reaction plane orientation (cos(PCW4)) and the particle rapidity.